International Workshop on Advanced Polymer Science and Turbulent Drag Reduction

10 - 20 March 2008

Electric, Dielectric and Magnetic Properties of Polymer and Carbon Fillers

Masaru MATSUO

Graduate School of Humanities and Sciences
Nara Women's University
Nara 630-8263
J A P A N

Electric, Dielectric and Magnetic Properties of Polymer and Carbon Fillers

Masaru Matsuo

Graduate School of Humanities and Sciences, Nara Women's University,

Nara 630-8263, Japan

Tel/Fax: (81)742203462, E-mail address: m-matsuo@cc.nara-wu.ac.jp

I. Introduction

Polymers in their pure state are excellent electrical insulators; however polymers can be modified to be good electrical conductors by simply mixing them with good conductors. To give conductive properties to polymers, carbon black (CB), carbon fibers (CF) and carbon nanotubes (CNT) have been utilized as conductive carbon fillers. Among these electrically conducting composites, some composites prepared by CB-polymer and CF-polymer composites show a sharp resistivity increase when the temperature close with the polymer melting point. This phenomenon is so-called as positive temperature coefficient (PTC) effect[1]. The remarkable PTC effect was mainly observed for conductor-filled semi-crystalline polymers, especially for low molecular weight polyethylene (LMWPE). Because of a sharp increase in electrical resistivity, the PTC materials have a wide range of industrial applications. They can be used as self-regulating heaters, current limiters, over current protectors and resettable fuses. However, there are some application limits because of the several drawbacks of thermoplastic conductive composites. They are 1) the lack of reproducibility of electrical conductivity due to irregular structure changes in heating/cooling cycles; 2) the decrease of electrical resistivity at the temperature beyond the melting point, which is so-called as NTC (Negative Temperature Coefficient) effect; and 3) the slow response rate of PTC effect associated with an adverse effect on desired switching properties. To pursue the improvement, a lot of efforts have been done by trial and error and consequently ultra-high molecular weight polyethylene (UHMWPE) was found to be better to prepare composites with conductive filler than LMWPE[2-3]. The materials provide the rapid

increase and rapid decrease in electrical resistivity at a critical temperature under heating and cooling processes and they ensure the good reproducibility.

CNTs are long and slender fibers where the walls of the tubes are hexagonal carbon (graphite structure) and often capped at each end. It has attacted great interest from all over the world since the moment it appeared. CNTs possess superior mechanical, thermal and electric properties. The exceptional properties of CNTs with low density offer scope for the development of nanotube-reinforced composite materials. Many efforts have been made in development of high electric and high modulus materials by filling CNTs into polymers. However, the Young's modulus and tensile strength were improved only several tens of percent, when CNTs were admixed into melted polymers.

In the present paper, we shall introduce the great improvements for Young's modulus and electric conductivity of multi-wall carbon nanotubes (MWNTs) and UHMWPE composites prepared by gelation/crystallization by using decalin as solvent. Actually, the composite could be elongated up to 100 times. The Young's modulus and electric conductivity reached 58 *GPa* and 10^{-1} *S/cm*[4]. This tendency becomes more considerable by iodine-doped treatments[5].

The highly elongation provides the composite preparation with high modulus and high conductivity. However, the alignment of CFs and CNTs perpendicular to the film normal direction must be done under electric and magnetic fields. These methods were carried out to orient liquid crystal chain axes in the directions of electric and magnetic fields. A number of papers concerned with theoretical and experimental aspects have been published. This workshop is concerned with theoretical physics, and then firstly the detailed theoretical treatments are discussed for electric, dielectric and magnetic characteristics of polymer and carbon filler composites. The electric and magnetic fields acting on the anisotropy of the electric or magnetic susceptibility exert torques within a liquid crystal which may complete with the elastic torques determining its internal structure. A general method is presented for calculating the molecular orientation in equilibrium state and the process up to the state.

II. Electric and Magnetic Orientation of Carbon and Polymer Chain Axes

Electric field

The magnitude of the birefringence under low electric field may be expressed by the Kerr law which is represented as $\Delta n = KE^2$, in which Δn is the birefringence, E is the external field intensity, and K is the Kerr coefficient characteristic of the sample. The proportionality tends to deviate with increasing electric fields.   This phenomenon was analyzed for steady-state electric birefringence by using a model that electrical and optical polarizabilities have no symmetry and the permanent dipole moment have orientation.   The orientation energy due to the permanent dipole is linearly dependent on electric field strength, while the energy due to the induced dipole depends upon the square of the field strength. Based on the general concept[1-3], the molecular orientation of liquid crystal chain axes shall be discussed in stead of CF axes, since the CF dispersion solution shows dark and birefringence cannot be measured.

The molecular orientation of rigid chains of liquid crystal under electric field at the equilibrium (steady) state may be given by using Cartesian coordinate shown in Figure II-1(a), which is given by[1-6]

$$\omega(\cos\theta) = \frac{e^{-U/\kappa T}}{\int_0^{2\pi}\int_0^{\pi} e^{-U/kT}\sin\theta\, d\theta\, d\eta} \tag{II-1}$$

where k and T are the Bolzmann constant and the absolute temperature, respectively, and U is the potential energy under the applied electric filed E, which is given by

$$U = U_1 + U_2 \tag{II-2}$$

where

$$U_1 = \mu_1 E\sin\theta\cos\theta - \mu_2 E\sin\theta\cos\eta - \mu_3 E\cos\theta \tag{II-3}$$

and

$$U_2 = \frac{(\alpha_2-\alpha_1)}{2}E^2\sin^2\theta\cos^2\eta - \frac{(\alpha_3-\alpha_2)}{2}E^2\cos^2\theta - \frac{\alpha_2 E^2}{2} \tag{II -4}$$
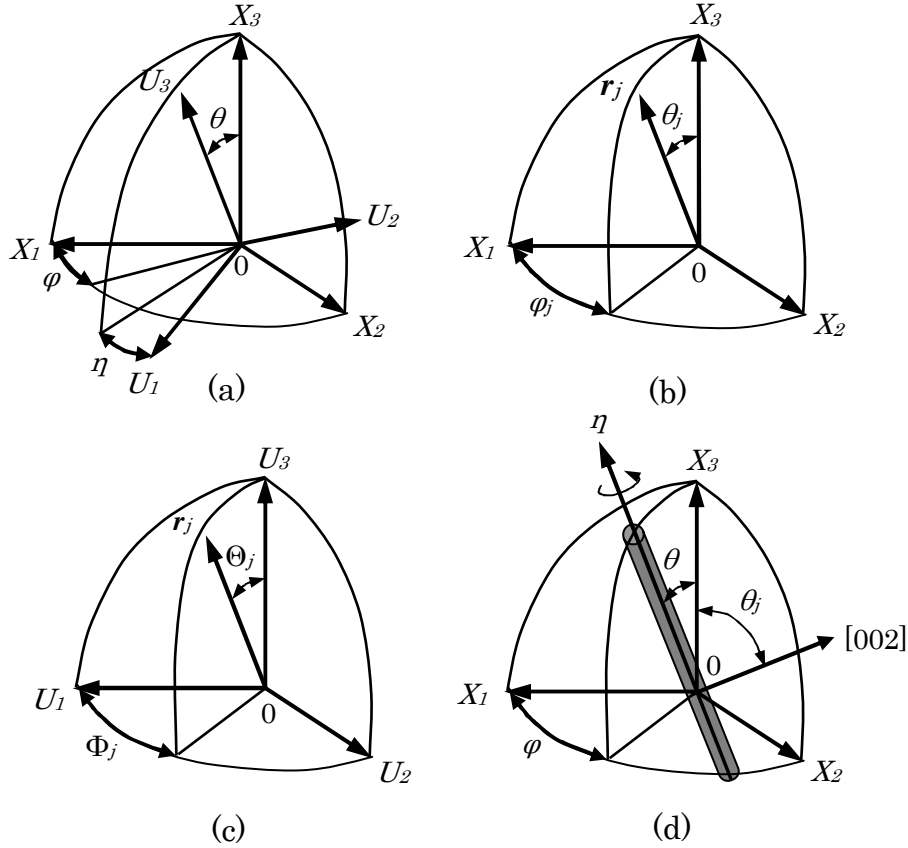
3

Figure II - 1. Cartesian coordimates illustrating illustrating the geometrical relation. (a) Euler angles θ and η which specify the orientation of coordinate $0\text{-}U_1U_2U_3$ of structural unit with respect to coordinate $0\text{-}X_1X_2X_3$ of specimen. (b) Angles θ_j and φ_j which specify the orientation of given j-th axis of the structural unit with respect to the coordinate $0\text{-}X_1X_2X_3$. (c) Angles Θ_j and Φ_j which specify the orientation of given j-th axis of the structural unit with respect to the coordinate $0\text{-}U_1U_2U_3$. (d) Geometrical arrangement of the reciprocal lattice vector of the (002) plane and fiber axis within the film coordinate $0\text{-}X_1X_2X_3$.

In Eq. (II-3), μ_3 is the apparent permanent dipole moment of molecular chain axis in solution, while μ_2 and μ_1 are the moments along the transverse direction of the chain axis. In Eq. (II-4), α_3 is the excess electrical polarizability along the chain axis, while α_2 and α_1 are the polarizabilities perpendicular to the chain axis.

The direct estimation of the molecular orientation function $\omega(\cos\theta)$ is very difficult under the applied electric field by X-ray diffraction measurement. The estimation has been done in terms of the second order moment of the orientation function $\omega(\cos\theta)$ by using birefringence measurement.

By assuming $\alpha_2 = \alpha_1$, the birefringence Δn may be given by[2]

$$\Delta n = \frac{4\pi^2}{n} C_V (g_3 - g_1) \int_0^\pi \omega(\cos\theta) \frac{3\cos^2\theta - 1}{2} \sin\theta d\theta \qquad \text{(II-5)}$$

where C_V = volume fraction of particles, n = index of refraction of the solution, $g_3 - g_1$ = optical anisotropy factor, g_3 and g_1 being the suffixes along the chain and the transverse direction.

As for the time to attend the equilibrium (steady) state, the orientation of CF axes are attributed to the rotation of the CF axes in the electric field direction. In this case, the distribution function $\omega(\cos\theta)$ may satisfy the following diffusion equation.[7-8]

$$\frac{\partial\omega}{\partial t} = \Theta\nabla^2\omega - div(\omega\frac{\tau}{\zeta}) \qquad \text{(II-6)}$$

where Θ is the rotational diffusion coefficient of polymer chain axes in the solution, τ is torque, ζ is the rotational fractional coefficient, and the symbol ∇^2 is the Laplacian operator. Θ is given by kT/ζ.

In order to carry out the solution of Eq. (II-6), the following parameters are defined as β (or b) and γ (or c) are given by

$$\beta = \frac{\mu}{kT}E = bE \qquad \text{(II-7)}$$

$$\gamma = \frac{(\alpha_3 - \alpha_1)}{2kT}E^2 = cE^2 \qquad \text{(II-8)}$$

An approximate solution of Eq. (II-6) can be obtained by using the perturbation method. By expanding λ_n and y_n in terms of E, we have

$$\lambda_n = n(n+1) + A_n E + B_n E^2 + C_n E^3 + D_n E^4 + - - - - - - - \qquad \text{(II-9)}$$

and

$$y_n(u) = P_n(u) + a_n(u)E + b_n(u)E^2 + c_n(u)E^3 + d_n(u)E^4 + - - - \qquad \text{(II-10)}$$

Subtracting Eqs. (II-9) and (II-10) into Eq. (II-6) and equating E, E^2, E^3, E^4, ---- to zero, we can obtain a set of ten differential equations. These equations are solved by

expanding $a_n(u)$, $b_n(u)$, $c_n(u)$, $d_n(u)$,----- in terms of Legendre functions.

The solution of Eq. (II-6) may be given by

$$\omega(u,t) = \sum_{n=0}^{\infty} A_n h_n \exp(-\lambda_n \Theta t) = \sum_{n=0}^{\infty} A_n y_n \exp\left(\frac{\beta u + \gamma u^2}{2}\right) \exp(-\lambda_n \Theta t) \qquad \text{(II-11)}$$

where $u = \cos\theta$ and A_n are the expansion coefficients. Incidentally, y_n must satisfy the following normalization condition.

$$\int_{-1}^{1} y_n^2 du = \frac{2}{2n+1} \qquad \text{(II-12)}$$

The electric birefringence is given by

$$\Delta(t) = \frac{4\pi^2}{n} C_V (g_3 - g_1) \int_0^{\pi} \omega(\cos\theta) \frac{3\cos^2\theta - 1}{2} \sin\theta d\theta \qquad \text{(II-13)}$$

Equation (II-13) is normalized by the birefringence $\Delta(\infty)$ for $t-> \infty$, i.e., the steady-state birefringence, which is given by

$$\Delta(t) = \frac{\Delta(t)}{\Delta(\infty)} \qquad \text{(II-14)}$$

In order to calculate Eq. (II-14), all the terms in the integrand must be expanded as a series of power for β, $\gamma \ll 1$. The calculation is carried out numerically.

The upper and lower parts in Figure II-2 terminated up to 4th order perturbation shows the normalized rise and reverse birefringence for various values of β^2 and γ reported already. The curves in Figure II-2 are very sensitive to the values of β^2 and γ. The birefringence becomes higher with increasing Θt and tends to level off. When inverse electric field is applied, the birefringence decreased and tends to level off.

The upper and lower sides in Figure II-3 show the corresponding birefringence at various electric field strength calculated by using $b = 2.27 \times 10^{-2}$ and $c = 5.16 \times 10^{-6}$ which were measured for poly(γ-benzyl - glutamate) in chloroform, the concentration being about 11 vol%[5]. With increasing the electric field strength, it is impossible to obtain the rise and reverse birefringence at the initial stage when a rectangular pulse and a reversing pulse are applied. This indicates the necessary of calculation beyond the fourth-order perturbation. Anyway, the saturation of birefringence becomes faster with increasing E indicating perfect orientation of polymer chain axis.
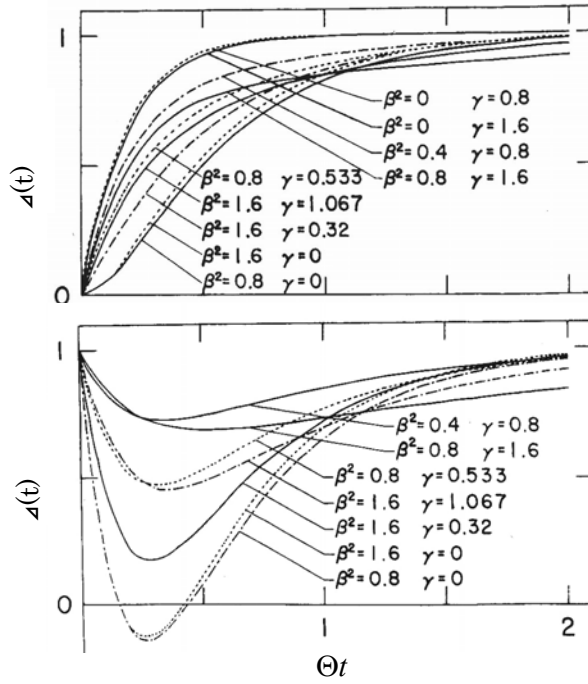
Figure II - 2. Normalized electric birefringence was Θt for various values of β^2 and γ, in which the upper and the lower are related to the rise and reverse field, respectively.
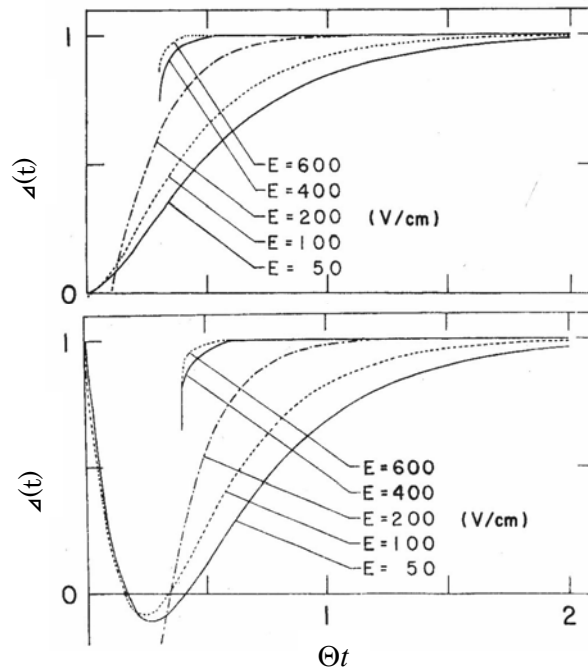

Figure II - 3. Normalized electric birefringence vs Θt calculated at $E = 200V/cm$, in which the upper and the lower are related to the rise and reverse field, respectively.

Magnetic field

The magnetic effect is proportional to the square of the magnetic flux density B and the origin of the diamagnetism is the induced magnetization caused by the induced motion of electrons under the applied magnetic field.[9-23] That is, the magnitude of the magnetization M induced on a material is proportional to the applied strength H, i.e., $M = \chi H$, where χ is the diamagnetic susceptibility. The interaction of M with the applied field causes a repulsive force, repelling the particle away to the direction of a decreasing field strength. If the force is equivalent to the gravitational force, the particles levitates in the air. Accordingly, when a material has an anisotropy in diamagnetism, a magnetic torque acts on it without the rotation. The origin of the magnetic anisotropy is traced back to chemical bonds. The magnetic anisotropy due to chemical bonds provides that diamagnetic susceptibilities of the C-C bond along the bond (//) are smaller than those perpendicular to the bond ($\perp$). Accordingly, the anisotropic diamagnetic susceptibility defined by $\chi_{//} - \chi_{\perp}$ ($\chi_{//} < \chi_{\perp} < 0$) is negative and then the C-C bond tends to align in the direction perpendicular to the applied field[23]. Here it may be noted that the orientation of the particles under magnetic field needs their volume to ensure energy higher than thermal disturbance associated with thermal energy.

The orientation of crystallites and particles under electric and magnetic field have been evaluated in terms of the second order orientation factor. The orientation under magnetic fields is related to the apparent permanent dipole moment, while that under electric field, the orientation is due to the excess electrical polarizabilities along symmetry and transverse axes in addition to the apparent permanent dipole moment. The comparison between theoretical and experimental orientations was done by birefringence[7, 24-25]. However, the orientation factor obtained by birefringence is a sort of the second moment of the orientation function.

The preferential orientation of carbon fibers within polymer matrix has been realized by elongation of the composite films[26]. Actually, carbon nanotube and ultra-high

molecular weight polyethylene (UHMWPE) composites could be elongated more than 100 times, when the composites were prepared by gelation/crystallization and the drawn composites provided high electric conductivity and high modulus. However, the ultra-drawn method is no effective to obtain the composites where the carbon fibers and carbon nanotubes are oriented predominantly with respect to the film normal (thickness) direction. To realize the preferential orientation, magnetic and electric fields must be applied to the direction parallel to the film thickness direction.

The orientation of carbon fibers[11-12] and carbon nanotubes[13-17] under the magnetic field has been evaluated from the two methods. One is the direct observation by scanning electron microscopy (SEM)[13], the other is due to the prediction of orientation of the reciprocal lattice vector of the (002) plane within the graphite crystal unit[17]. The measurements were done for the composite film prepared by evaporating solvents from polymer gels.

In the present paper, PVA-CF composites were prepared by gelation/crystallization from solutions in dimethyl-sulfoxide (DMSO) and water mixtures. The polymerization of PVA was ca. 2000. The DMSO/water composition was set to be 60/40, assuring rapid gelation and stiff gel reported elsewhere[27]. The contents of CFs against the mixed solvent were 0.3, 0.5, 1.0 and 2.5%, in which the concentration of PVA against the mixed solvent was fixed to be 10g/100mL. To obtain further information for the viscosity dependence of PVA, 13g/100mL solution was prepared, in which the CF content against the mixed solvent was 1.0%.

The short carbon fibers used in this experiment are MGII from Toho Tenax Co. Ltd, the average size of which was $\varnothing$ 15μm × 80 μm. The length distribution is scattered from 4μm to 150μm. The carbon fibers were made from the carbonization of polyacrylonitrile (PAN). The conductivity was ca. 700 S/cm.

Figure II-4 shows the specific viscosity against PVA concentration. The viscosity increases drastically with increasing PVA content. This data is important to pursue theoretical calculation of the orientation distribution function of the CFs. Unfortunately,

the measured values of η_{sp} were too scattered to obtain the creditable values, when the CFs were admixed into PVA solution. But the CF contents, 0.3 ~ 2.5% at the 10% PVA solution (against the solvent) concentration were confirmed not so sensitive to the η_{sp} values. Any drastic increase in η_{sp} values did not occur.
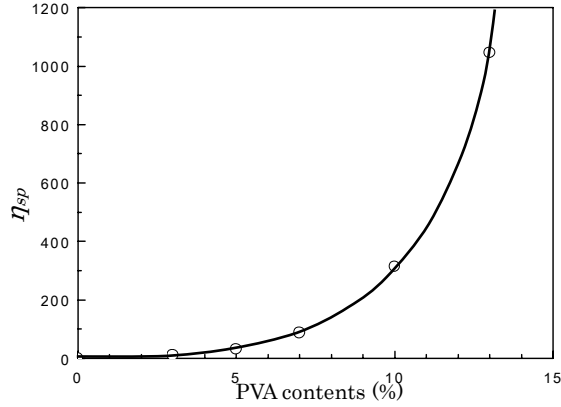

Figure II - 4. The specific viscosity η_{sp} of PVA solutions with

The magnetic orientation of carbon fiber with susceptibility anisotropy at the equilibrium state may be estimated by the concept similar to the theory of the electric field. Then the orientation function of the carbon fiber axes are given by the same equation as described in Eq. (II-1).

However, in the magnetic field, U is the magnetic energy under the applied magnetic flux density B ($= (1 + \chi)H$), in which $U_1 = 0$ and U_2 may be rewritten as

$$U = -\frac{\left(\chi_{\parallel} - \chi_{\perp}\right)B^2 V \cos^2 \theta}{2\mu_0} - \frac{\chi_{\perp} B^2 V}{2\mu_0} \tag{II-15}$$

where μ_0 and V are the magnetic permeability of vacuum and the volume of the particle under consideration, and $\chi_{//}$ and $\chi_{\perp}$ are the anisotropic susceptibilities parallel and perpendicular to the carbon fiber. θ is the angle between the carbon fiber and the applied magnetic field directions. Generally, it may be noted that a macroscopic orientation can occur when the first term exceeds the thermal energy kT represented as $V > 2kT\mu_0|\chi_{//} - \chi_{\perp}|B^2$. This indicates that there exists the estimation of minimum

critical volume V needed for the orientation given as a function of the applied magnetic flux density B and the difference $|\chi_{//} - \chi_{\perp}|$ between anisotropic susceptibilities parallel and perpendicular to the carbon fiber.

Substituting Eq. (II-15) into Eq. (II-1) to calculate the orientation function $\omega(\cos\theta)$ of the carbon fibers, the second term on right hand in Eq.(II-15) is independent of the profile of $\omega(\cos\theta)$. Then, Eq. (II-1) may be given by

$$2\pi\omega(\theta) = \frac{e^{\gamma\cos^2\theta}}{\int_0^\pi e^{\gamma\cos^2\theta} \sin\theta d\theta} \qquad \text{(II-16)}$$

where

$$\gamma = (\chi_{//} - \chi_{\perp})\frac{V}{2\mu_0 kT}B^2 \qquad \text{(II-17)}$$

The orientation of CF axes are attributed to the rotation of the CF axes in the magnetic field direction. In this case, the distribution function $\omega(\cos\theta)$ may satisfy the same diffusion equation as Eq. (II-6). τ is given by

$$\tau = -\frac{(\chi_{\parallel} - \chi_{\perp})V}{\mu_0}B^2 \sin\theta\cos\theta \qquad \text{(II-18)}$$

Here, the general solution of Eq. (II-6) under the magnetic field is given by

$$\omega(u,t) = \sum_{n=0}^\infty W_n h_n \exp(-\lambda_n\Theta t) = \sum_{n=0}^\infty W_n y_n \exp\left(\frac{\gamma u^2}{2}\right)\exp(-\lambda_n\Theta t) \qquad \text{(II-19)}$$

where W_n are the expansion coefficients and they are determined so as to satisfy the initial condition.   Eq. (II-19) for the magnetic field is much simpler than Eq. (II-11) for the electric field.

Here it may be noted that the second order orientation factor $F_{200}(t)$ and the average angle $\overline{\theta}(t)$ as a function of time can be obtained by using Eq. (II-19), as follows:

$$F_{200}(t) = \left[\frac{3<\cos^2\theta>-1}{2}\right]_t = \left[\frac{3<u^2>-1}{2}\right]_t = \int_{-1}^1 \frac{3u^2-1}{2}\omega(u,t)du \qquad \text{(II-20)}$$

and

$$\bar{\theta}(t) = \int_0^\pi \theta\omega(\cos\theta, t)\sin\theta d\theta \qquad \text{(II-21)}$$

Since a CF is surely a rigid cylinder like tobacco-mosaic virus, Θ may be given by[28]

$$\Theta = \frac{3kT}{8\pi\eta_0 a^3}\left[\ell n 2p - 1.57 + 7\left(\frac{1}{\ell n 2p} - 0.28\right)^2 \pm 0.2^5\right] = \frac{kT}{\zeta} \qquad \text{(II-22)}$$

where a is an average half length of CFs and p is an average aspect ratio. η_0 is viscosity of the CF dispersed PVA solution. To pursue the numerical calculation, Θ .

Figure II-5 shows the orientation distribution functions calculated at the indicated values of Θt for the indicated four CF contents dispersed in 10% PVA solution. The theoretical calculations for the indicated dispersion solutions were done by using the same γ value associated with each equilibrium state. The termination error up to the 10-th order perturbation did not give any problem for the numerical calculation and the calculated distribution functions become almost stable. The curve profile calculated at the indicated CF contents becomes sharper with increasing Θt and is equal to the corresponding saturated curve. Namely, the calculated curve profile with a maximum value at $\theta = 0^o$ become sharper with elapsing time. This means that the orientation of CFs tends to orient gradually with elapsing time. Here we must emphasize that the estimation of CF magnetic orientation in terms of the distribution function is very important in comparison with the average estimations representing by Eqs. (II-20) and (II-21). Because the distribution function represented by Eq. (II-19) only reveals actual orientation behavior.

Here it should be noted that the γ value represented by Eq. (II-17) is essentially independent of the CF content and then the saturation time must be the same. Also the value of the rotational diffusion constant Θ must be almost the same, since the admixture of CFs up to 2.5% was confirmed not so sensitive to the change in viscosity η_o of the solution. As discussed before, the large difference at the 2.5% CF content is probably thought to be due to the collision between adjacent CFs under the magnetic

field. In contrast, the CFs can be oriented without any disturbance between adjacent CFs at 0.3, 0.5 and 1.0% contents. This indicates that at 2.5% content, the disturbance by the collision is very serious to promote the magnetic orientation degree.
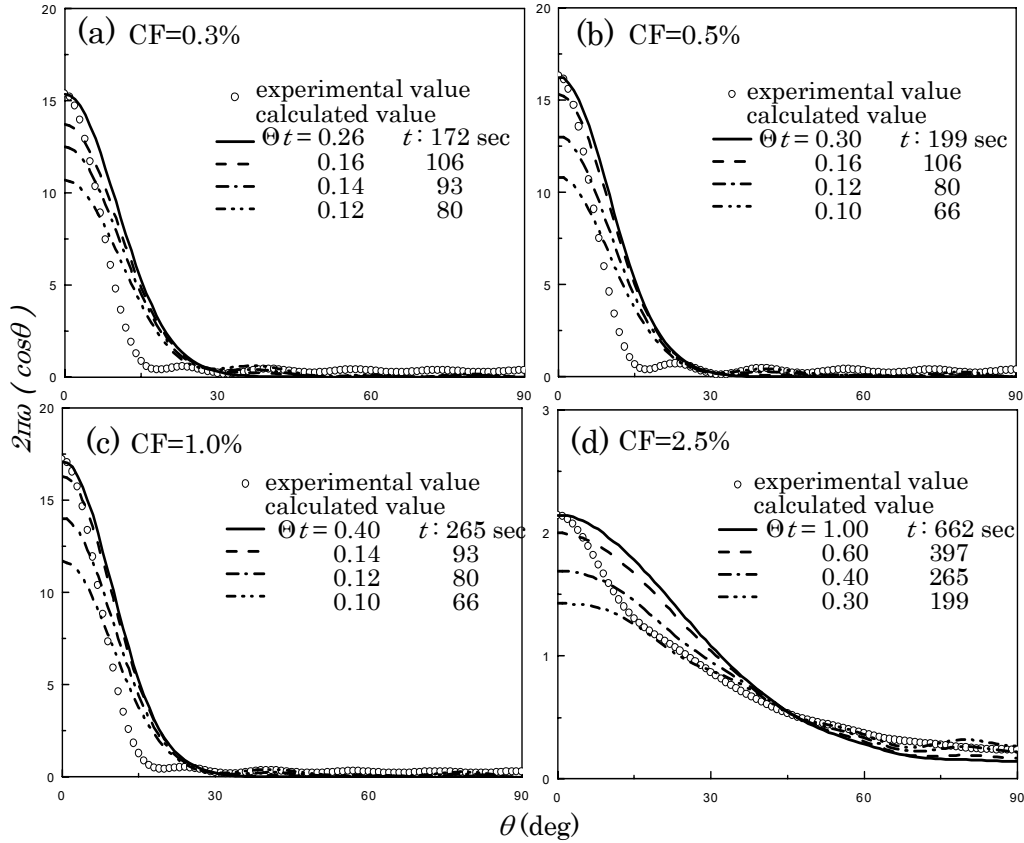

Figure II - 5. $2\pi\omega(\cos\theta)$ of carbon fiber axes in the composites prepared from 10% PVA solution containing the indicated CF contents. Open circles are experimental values and solid curves are calculated on the basis of Eq. (6) in which the γ are given (a) 16.013, (b) 16.846 (c) 17.745 and (d) 2.730.

In Figure II-5, t is the period corresponding to Θt and the value is calculated by Eq. (II-15). In the calculation, the average half length a_0 of CFs and the average aspect ratio p are given as 33.3 μm and 6.924, respectively. The viscosities η_0 at 10 and 13% PVA solutions are given as 2.241 and 7.547 poise, respectively. The values of t to reach their saturation state at 0.3, 0.5 and 1.0% CF are calculated to be 172, 199 and 265 sec, respectively. This indicates that the calculated saturation period becomes longer with increasing CF content, although the γ value differences among the three CF contents are very small. The CF content dependence of the saturation period may be rigorous

13

because of fewer possibility of the collision between neighbor CFs under the magnetic orientation.

Figure II-6(a) and (b) show the orientation distribution functions calculated at the indicated values of Θt. The calculations were carried out for 10 and 13% PVA solutions containing 1.0% CF content. The column (a), appeared in Figure II-5(c), is shown again to compare the two curve profiles each other. Of course, the calculation was done for the indicated dispersion solutions by using the same γ value indicating the equilibrium state in Figure II-4. The curve at 13% PVA concentration is duller than that at 10% PVA. This result also indicates that the high viscosity of solution due to an increase in PVA content hampers the magnetic orientation of CFs. Judging from Figure II-4, the magnetic orientation of CFs in 13% PVA solution becomes poorer than that in 10% PVA solution in spite of the same CF content. This is attributed to the decrease of Θ proportional to the reciprocal value of viscosity η_o as represented in Eq. (II-22). The predicted period up to the equilibrium state is 662 sec.
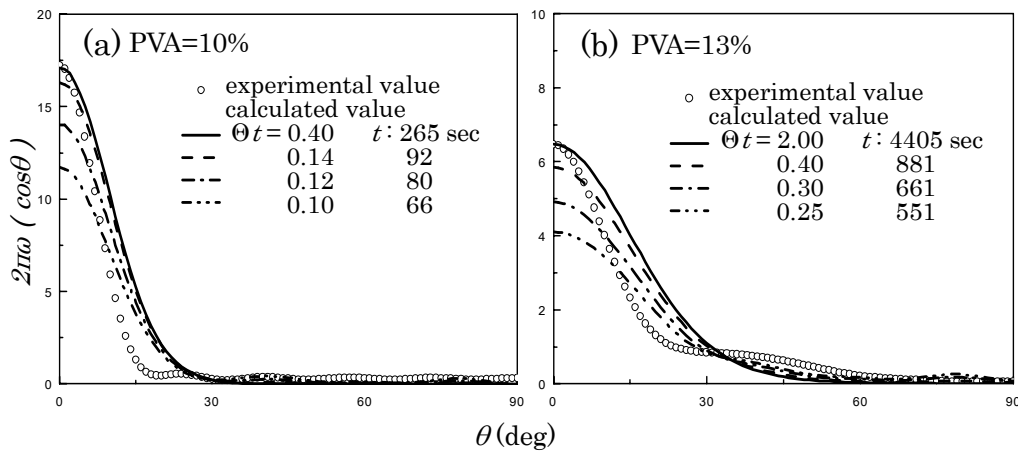

Figure II - 6. $2\pi\omega(\cos\theta)$ of carbon fiber axes in the composites prepared from 10 and 13% PVA solutions with 1.0% CF content. Open circles are experimental values and solid curves are calculated by Eq. (6), in which γ are given (a) 17.745 and (b) 7.093.

In Figure II - 6, the saturation time of the orientation of CF axes at 13% PVA solution becomes longer than that at 10% PVA solution. It takes more than 1h because of very high viscosity of the solution as shown in Figure II-4.

Figure II-7 (a) and (b) show the second order orientation factor $F_{200}(t)$ and the average angle $\bar{\theta}(t)$, respectively, for 0.3, 0.5, 1.0 and 2.5% CF contents dispersed in 10% PVA solution. As shown in column (a), the factor becomes unity for perfect orientation of the CF axes with respect to the film normal direction (magnetic field direction), while it becomes zero for the random orientation. The factor increases drastically with increasing Θt and tends to level off. This tendency is almost the same as the behavior of the dispersed solutions with 0.3, 0.5and 1.0% CF contents. On the other hand, the factor for the 2.5% CF content increased gradually. This indicates that the low value of $F_{200}(t)$ and slow time up to the steady state are due to the drastic collision between adjacent CFs under magnetic orientation and the magnetic field used in the present work is too low to enhance the orientation of the CF axes in the dispersion solution containing 2.5% CF content.
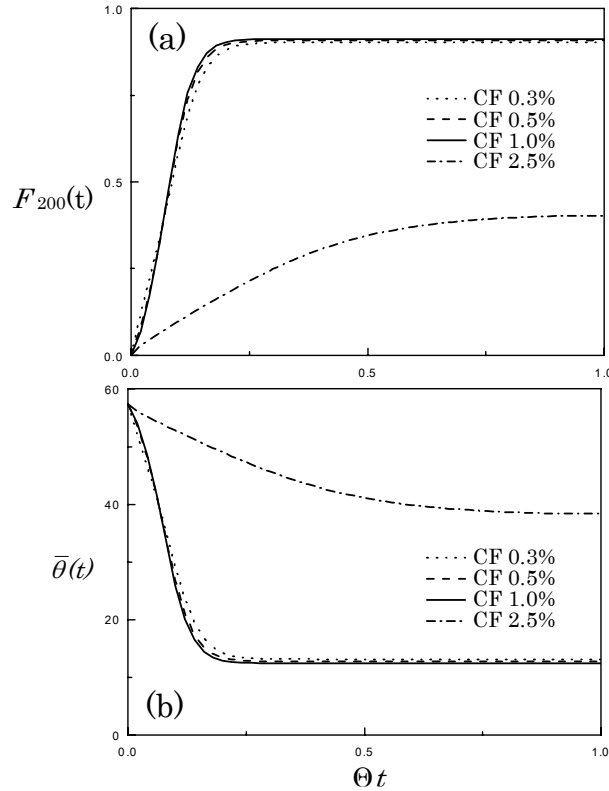

Figure II - 7. (a) The second order orientation factor calculated by Eq. (6) and (b) the average angle for the composites prepared from 10% PVA solution containing the indicated CF contents.

The average angle $\bar{\theta}(t)$ becomes lower with increasing Θt and tends to level off for 0.3, 0.5 and 1.0% CF contents dispersed in 10% PVA solution, indicating the progression of the orientation of the CF axes. On the other hand, the orientation for the 2.5% CF content is not so significant.

Figure II-8(a) and (b) shows the estimation second order orientation factor $F_{200}(t)$ and the average angle $\bar{\theta}(t)$, respectively, for 10 and 13% PVA solution containing 1.0% CF. The results in columns (a) and (b) indicate that the increase in PVA concentration causes drastic increase in viscosity and the orientation of CF axes becomes less pronounced.
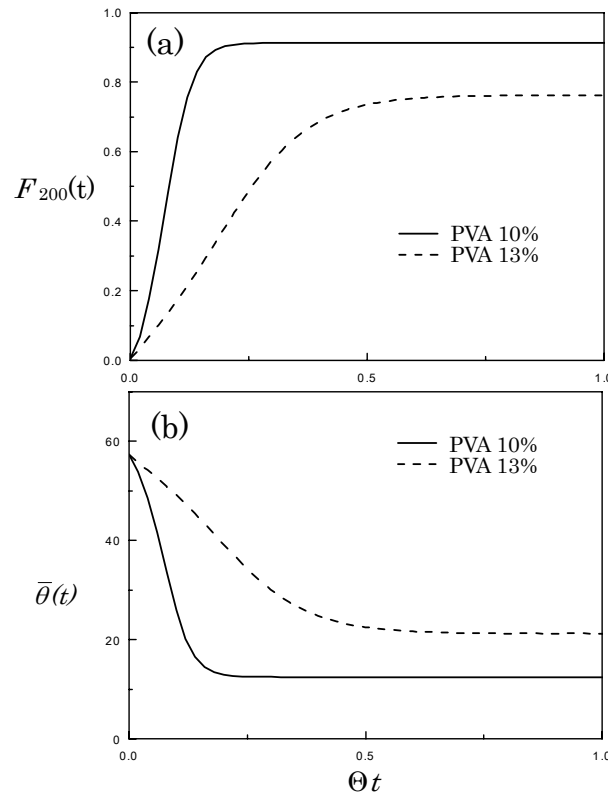

Figure II - 8. (a) The second order orientation factor calculated by Eq. (6) and (b) the average angle for the composites prepared from 10 and 13% PVA solutions with 1.0% CF content.

The second order orientation factor and the average angle in Figures II-7 and 8 provide simple representation to facilitate easy understanding. Even so, the detailed phenomenon must be evaluated in terms of the orientation distribution function. As shown in Figures II-7 and 8, the saturation values of Θt estimated by $F_{200}(t)$ in Figure

II-7 are almost 0.25 for the 0.3, 0.5 and 1.0% CF contents but the corresponding value of Θt estimated by $\omega(\cos\theta)$ are 0.26, 0.30 and 0.40, respectively as shown in Figure II-5. This means that the estimation by $\omega(\cos\theta)$ is much better to pursue precise estimation for the orientation behavior of CF axes under magnetic field.

$\bar{\theta}(t)$ is close to 10° at the saturated state of the CF orientation but the most probable density of CF axes is not maximum at 10° and it must be 0° as shown in Figures II-5 and 6. To avoid such a contradiction, the orientation function must be adopted. Unfortunately, the orientation function can be only obtained by X-ray diffraction technique. But, as discussed elsewhere[5-7, 24-25], the estimation is very difficult for solution and liquid crystals under electric and magnetic fields. Most of the estimations have been carried out by birefringence measurements associated with the second order orientation factor. In the present work, of course, it was very difficult to evaluate of CF axes in solution under the magnetic field by X-ray diffraction technique, and then the estimation was done for the composites on the basis of the assumption that the same orientation degree of CF axes in the dispersed solution is maintained in the bulk specimen proposed by gelation/crystallization and then evaporating the solvent from the gels. Namely, any change in the orientation degree of the CFs under the magnetic field does not occur under evaporating process of the solvent.

Incidentally, electric conductivities of the present PVA-CF composite films are hardly affected by the magnetic orientation of CFs and the values were ca. 10^{11} S/cm indicating the original conductivity of PVA films. The orientation of large amount of CFs must be carried out under high magnetic field to prepare PVA-CF composites with anisotropic electric conductivity.

In this paper, it is necessary to derive the orientation function of CF axes from the orientation of the reciprocal lattice vector of the (002) plane of graphite crystal. The derivation is not son difficult but the mathematical background for analyzing the orientation distribution function of crystallites[29-41].

III. Electric and Dielectric Properties of Polymer-Carbon Fiber Composites

Most of polymers are typical insulators. To give conductive properties to polymers, carbon black (CB)[1-9] carbon fibers (CF)[10-11] and some metal powders[12] have been utilized as conductive filler. Among these electrically conducting composites, some composites show a sharp resistivity increase when the temperature close with the polymer melting point. This phenomenon is so-called as positive temperature coefficient (PTC) effect. In order to explain PTC mechanism, several theories have been proposed. Some of them are percolation phenomenon, conduction pathway theory, thermal expansion theory, tunnel effect theory and electric field emission theory[1-2, 13-16], etc. Nevertheless, these theories still remain some problems to explain experimental results clearly.

This chapter deals with some approaches to investigate electric and dielectric properties of ultra-high molecular weight polyethylene (UHMWPE)-CF composites prepared by gelation/crystallization from solutions.

The samples were prepared by using UHMWPE (Hercules 19000/90189) with an average viscosity molecular weight of 6×10^6, LMWPE (Sumikathene G201) with an average viscosity molecular weight of 4×10^4.

The concentrations of UHMWPE and LMWPE against decalin were fixed at 0.5g/100ml and 4.5g/100ml respectively. Namely, for the blend film, the weight composition (LHWPE/UHMWPE) was 9/1. The hot homogenized solution was quenched by pouring it into an aluminum tray at room temperature, thus generating a gel. The decalin was allowed to evaporate from the gel under ambient conditions. The nearly dry gels were vacuum-dried for 24 hours to remove residual traces of decalin. The weight compositions of CF and UHMWPE of the blends were varied by 0.5/1, 1/1, 2/1, 3/1, 4/1, 5/1, 6/1, 7/1, 8/1. The corresponding CF volume contents calculated against the matrix are 2.1%, 4.2%, 8.0%, 11.6%, 15.0%, 18.0%, 21.0%, 23.5%, 26.0%.

Figure III-1(a) shows the electrical resistivity as a function of fiber volume content at

room-temperature. A zigzag drop in resistivity against carbon fiber content is observed, which is generally attributed to percolation phenomenon. At lower fiber contents (2.1~11.6 vol%), the resistivity is more or less equal to the resistivity of pure polymer.
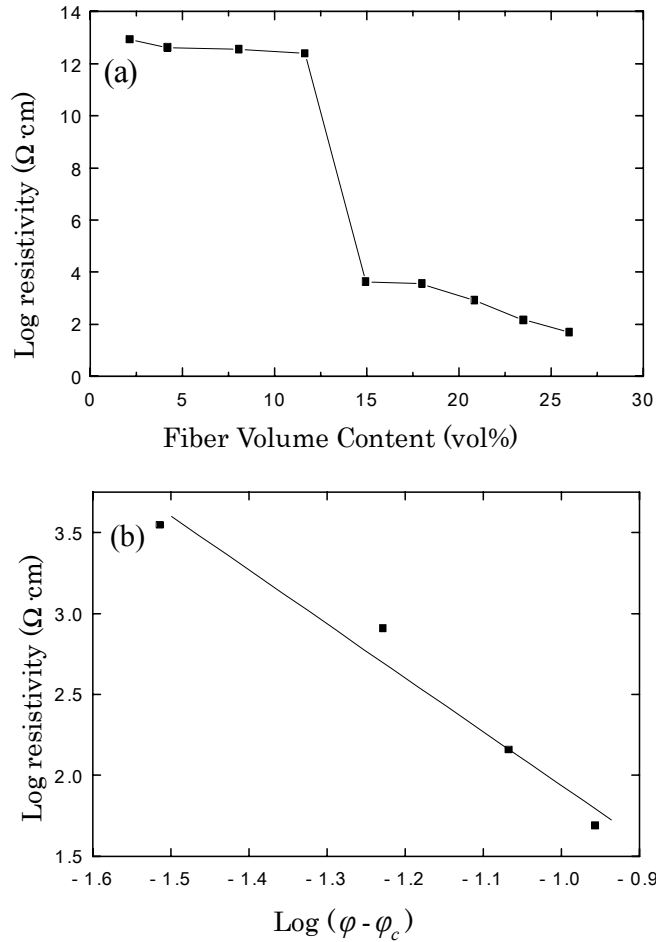

Figure III -1.   (a) Electrical resistivity versus volume fraction of carbon fibers; (b) Log-log plot of the resistivity against $\varphi - \varphi_c$ with $\varphi_c = 15.0\%$ according to Eq. IV-1. Straight line was plotted by least-square method and has a slope $t = 3.32$

When carbon fiber content increases to 15.0 vol%, the resistivity of the blends falls down sharply from 10^{12} to 10^4 Ω·cm, indicating the electrical conversion of composites at a critical concentration of carbon fibers. A semiconducting character of the composites in this transition region can be explained by a specific conductance mechanism of these materials. Namely, it may be expected that even if a few conducting paths are present,

electrons are activated to hop over the nonconducting polyethylene matrix barrier across the gaps between the conducting fibers. When carbon fiber content exceeds the critical concentration, the conduction is predominantly achieved through the fiber contacts and the material behaves as a conductor. The resistivity of composites tends to level off when CF content is beyond 15.0 vol%. As discussed already, the blends were mixed by putting all the components into the decalin solution at 150℃. This method allows more fillers in the blends to obtain the lower resistivity. At the same time, the percolation threshold value is higher than that of conventional conductive polymer blends produced by melt mixing of polymer and fillers, since carbon fibers can be uniformly dispersed and the interparticle distances are longer without kneading or pressing at high pressure.

Percolation theory predicts the relationship between the composite resistivity and volume content of the conductive filler as

$$\rho = \rho_0(\phi - \phi_c)^{-t} \quad \text{for} \quad \phi > \phi_c \qquad \text{(III - 1)}$$

where ρ_0 is a constant, ϕ is the volume content of the filler, ϕ_c is the critical volume content at percolation threshold, which is 15.0 vol% in the present paper, t is the exponent characterizing the relationship between ρ and ϕ. Theoretical consideration has provided that t should be equal to 1.5~1.6. However t value was given to be about 3 experimentally for the composite filled with randomly oriented fibers[10]. For the present composites, t value was determined to be 3.32 from the slop of line shown in Figure III-1(b).

In fact, the filler concentration of the desired composites serving as PTC materials should be a little bit higher than the upper limit value estimated by the percolation region [3-5, 29]. Accordingly, the sample, where the concentration is higher than or equal to 15.0 vol%, was chosen to test their PTC effects in the present chapter.

It has been pointed out that the thermoplastic composites exhibit poor reproducibility of resistivity-temperature curves for different heating/cooling runs. According to previous reports, poor reproducibility of electrical conductivity could be a little

improved by cross-linking either chemically with peroxides or by irradiation[4], and by adding rubber as a "mechanical stabilizer" to carbon black/wax mixtures[30] and by using mixtures of two kinds of carbon black with polyethylene[3]. This is obviously due to the fact that the expansion/contraction processes accompanying heating/cooling cycles cause movements of the fillers and the behaviors is irreversible. However, in the case of the blends with UHMWPE[8-9,18,31], the reproducibility of electrical conductivity provided good satisfication, since UHMWPE minimizes the migration of the carbon fibers and the deformation because of its high viscosity even in the temperature range beyond the melting point. Only the first run is different from the subsequent ones, while the latter runs have very good reproducibility shown in Figure III-2. As the most favorable phenomenon in the latter run, the resistivity increases abruptly at sharp temperature range about 116℃. It is noticed that the latter curves shifted upward and forward in comparison with the first run because of the decrease of crystallinity for both UHMWPE and LMWPE after the first runs.
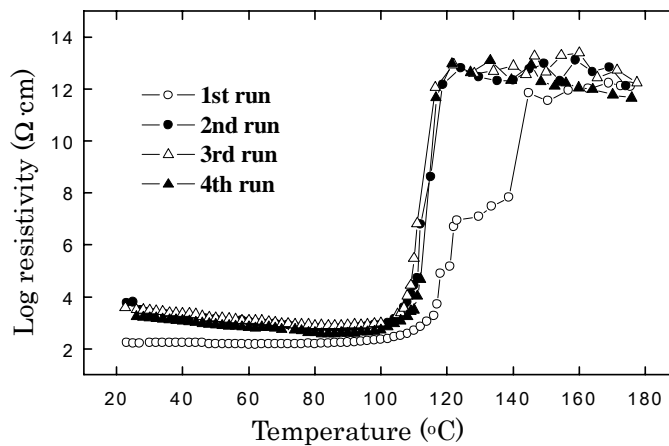

Figure III - 2.   Resistivity against temperature of the 90/10 w/w LMWPE/ UHMWPE blends with 23.5 vol% CF under four runs

Figure III-3 shows the resistivity of the blends with the different volume content as a function of temperature. The results indicate that the PTC effect is dependent on the carbon fiber content. At highest content (26 vol%), the PTC effect of the composites becomes worst. At lower contents (15.0 vol% ~18.0 vol%), the PTC intensity is about

21

10^6 and the PTC temperature is about 100℃. When the volume content is 23.5 vol%, the PTC intensity reach a maximum about 10^9 and the PTC temperature is about 116℃. The reason maybe is due to the fact that the smaller inter-fiber distance in the composites becomes narrower with increasing CF content and the higher temperature is required to break off all contacts of carbon fibers.
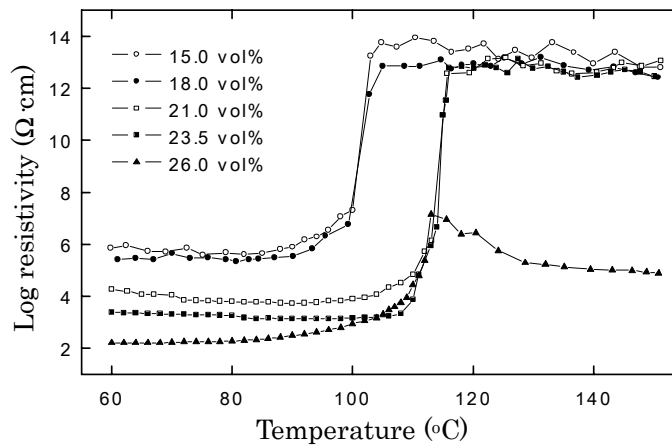

Figure III - 3 Resistivity against temperature of the blends with the different CF content

The results of the other research[3-5, 29] indicated that only when a filler concentration is a bit higher than the upper limit of the percolation region, the material with PTC effect can be achieved. Furthermore, if a high conductivity is required, highly filled composites should be employed for switching purposes. Such highly conductive composites, however, seldom show good switching behavior. Therefore, the composites combining high conductivities and significant switching behavior are a contradictory. Nevertheless, in the 90/10 w/w LMWPE/UHMWPE blends with carbon fibers, the PTC effects can be found in a wide concentration range from 15.0 to 23.5 vol%, which has never been reported in the previous literature[3-5, 7-9, 29].

However, the composites prepared by using carbon fibers, which have the electrical conductivity similar to carbon blacks, as conductive fillers have seldom attracted the attention of the researchers. In previous paper[32], we reported a new PTC composite by using blends of ultra-high molecular weight polyethylene (UHMWPE) and low

molecular weight polyethylene (LMWPE) filled with short carbon fibers, prepared by the gelation/crystallization from dilute solution, in which LMWPE/UHMWPE composition was 9/1 and carbon fiber content within the blend was 23.5 vol%. The new composite provided a drastic excellent PTC effect showing very sharp increase in electrical resistivity at 116oC and no NTC effect beyond the melting point.

Based on the successful results in the previous paper[32], the present paper deals with the origins of PTC and NTC effects of short carbon fibers in polyethylene matrix by considering a model system composed of random arrays of closely spaced conductors dispersed in an insulating polymer matrix. The application is done for a simple resistor-capacitor circuit model to explore the interface relaxation between carbon fibers and polyethylene matrix, the AC conductivity and dielectric permittivity behavior of the composites. In doing so, broad frequency measurements were adopted to probe the conducting path and the space gaps, in order to show the experimental evidence for explaining PTC mechanism as well as to emphasize that the impedance spectroscopy can be used as a tool to analysis the dispersion of the carbon fillers or other conductive fillers. This method may provide further important information to promote the PTC effect by developing several conductive carbon fillers.

When the concentration of carbon fiber is high enough, a continuous carbon network is formed in the solid polymer matrix. As we know, the electron tunneling is a dominant transport process in carbon fiber-polymer composites, and the electrical conductance depends on the distance between neighbor carbon fibers. Hence the composites can be regarded as the system composed of random arrays of closely spaced conductors dispersed in an insulating polymer matrix. The degree of the contacts of the fibers may be varied according to the dispersion mode of the carbon fibers and the morphology of polymer matrix.

Similar to the resistor-capacitor circuit model of carbon black-polymer system suggested by Kawamoto[36], the resistor-capacitor circuit model of carbon fiber-polymer system was proposed in Figure III-4a. In this model system, the two possible electrical

current components, competing with each other in a contact region between carbon fibers, are considered; one is a current through an internal contact resistor R_c, and the other is a current through a contact capacitor C_c. R_a represents the resistance of carbon fibers which is held very tight.
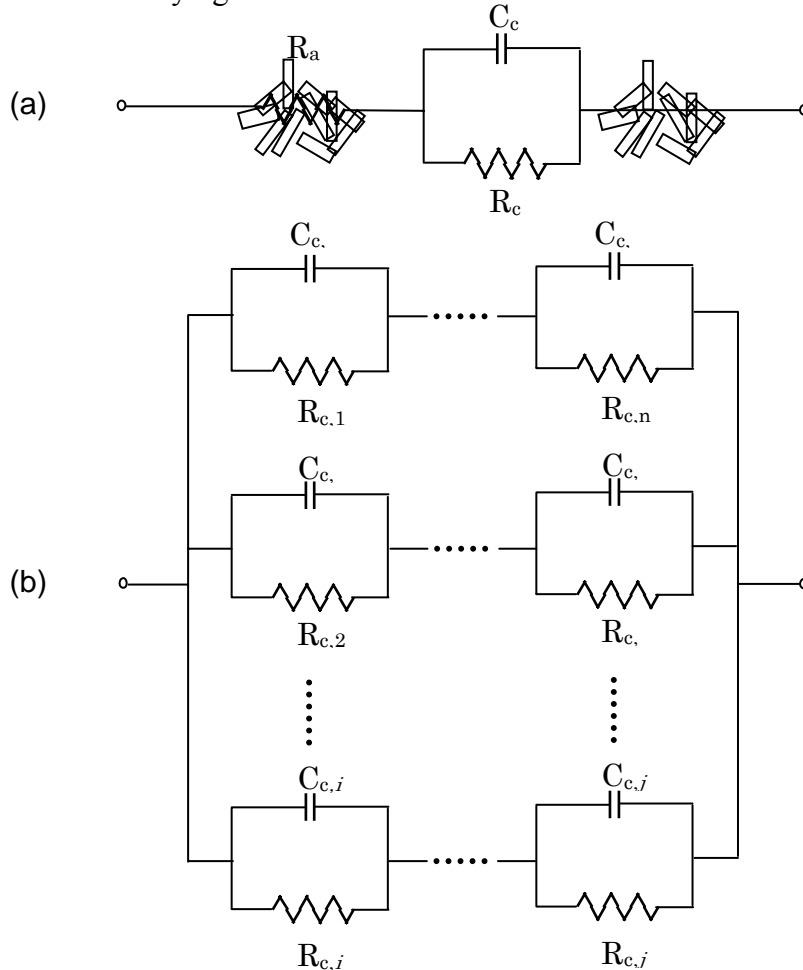

Figure III -4. Circuit models of carbon fibers: (a) simple resistor-capacitor circuit in the contact region of carbon fibers, (b) Equivalent resistor-capacitor parallel circuit

At low temperatures, the electrical current tunneling through the fiber network with negligible direct contact between fibers (Rc) is thought to be principal. At higher temperatures, it is evident that the R_c increases due to the thermal expansion of the matrix between fibers, and at the same time, the component of contact capacitors with a strong dependence on frequency increased. The electrical current is not only depending on temperature but also depending on AC frequency of electrical signals (DC is viewed

as infinite in time). Under this assumption, we will observe mainly the AC electrical response of the polymer blend located between the fiber interface regions.

If the carbon fibers which are held very tight can be considered as pure resistive, the simplified equivalent circuit model will be adopted as shown in Figure III-4b. The current components in the composite can be analyzed by an impedance analyzer.

For a given frequency, the complex impedance $Z*$ is given by

$$Z* = Z' + iZ'', \qquad i = (-1)^{1/2} \tag{III-2}$$

where the resistance Z' is the real part of the impedance, which is due to the current through the contact resistor, and the reactance Z'' is the imaginary part of the impedance, which is due to the current through the contact capacitor. Z' is equal to resistance R if the frequency is zero or DC measurement. The conductance of the equivalent circuit can be written as

$$G* = \frac{1}{Z*} = G' + i\omega C \tag{III-3}$$

where G' is the AC conductance and C is the capacitance at zero frequency. The AC conductivity σ_{AC} is equal to G' modified by geometric factor of the sample.

The corresponding complex permittivity $\varepsilon* = \varepsilon' - i\varepsilon''$ can be written by

$$\varepsilon' = \frac{1}{\omega C_0} \frac{-Z''}{Z'^2 + Z''^2} \tag{III-4}$$

$$\varepsilon'' = \frac{1}{\omega C_0} \frac{Z'}{Z'^2 + Z''^2} \tag{III-5}$$

where C_0 is the geometric capacity $(= \varepsilon_0 \frac{S}{d})$, ε_0 is the vacuum permittivity, and S and d are the area and thickness of the sample, respectively.

Complex modulus $M*$, which is the inverse complex permittivity, is defined by

following equation

$$M* = \frac{1}{\varepsilon*} = \frac{1}{\varepsilon' - i\varepsilon''} = \frac{\varepsilon'}{\varepsilon'^2 + \varepsilon''^2} + i\frac{\varepsilon''}{\varepsilon'^2 + \varepsilon''^2} = M' + iM'' \qquad \text{(III-6)}$$

where M' and M'' are the real and the imaginary electric modulus, respectively.

The PTC effect of DC conductivity was reported. Figure III-5 shows the dependence of AC conductivity as a function of the frequency at indicated temperatures. In the vicinity of 116 °C, the similar PTC effect in AC conductivity of the composite also can be observed, which would be discussed in details in Figure III-7 later.
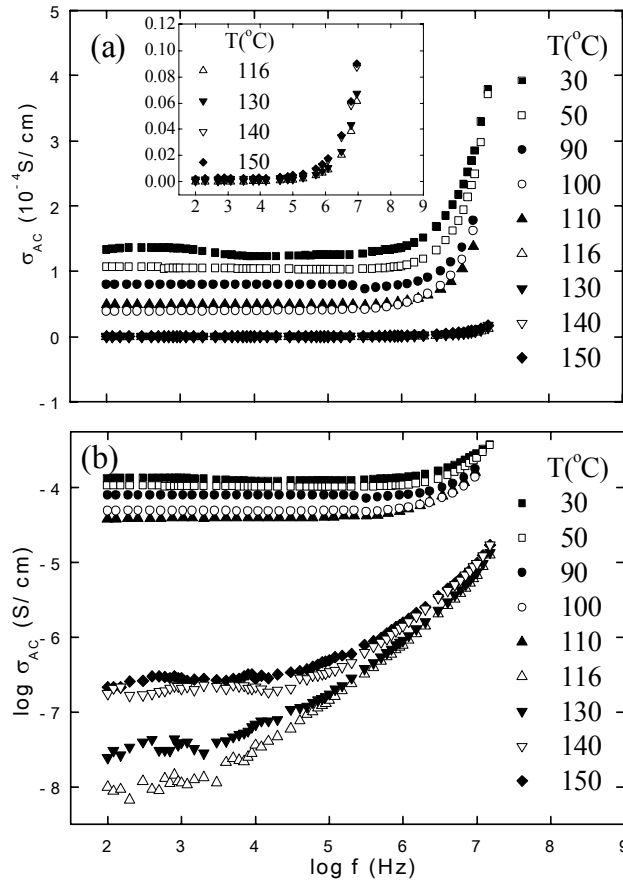

Figure III -5. The AC conductivity versus log f at various temperatures: (a) σ_{AC} and (b) $\log \sigma_{AC}$. The inset is the magnification of the plots at temperatures higher than 116 °C

At low frequencies (below 10^5 Hz), we observed that the conductivity depended little on frequency. This phenomenon could be attributed to resistive conduction through the

bulk composite including tunneling between fibers. On the other hand, at high frequencies (above 10^5 Hz), conductivity was proportional to frequency due to the capacitance of the matrix between the conducting particles or clusters.

The logarithm plots of conductivity σ_{AC} against frequency f shown in Figure III-5b reveal further AC behavior of the system. These frequency dependence curves can be clearly distinguished into two groups in Figure III-5b. The DC conductivity plateau means that the conductivity is similar to that measured by a DC method. We maybe conclude that an infinite cluster is present at the temperatures lower than 116 ℃. With the increasing temperature and frequency, DC conductivity plateau disappeared and the AC conductivity became higher than DC conductivity. It can be assumed that the conduction networks of carbon fibers are broken and both DC and AC conductivity drop drastically as a result of thermal expansion of polymer matrix. According to the resistor-capacitor circuit model, the amount of direct contacts between carbon fibers is decreased by the volume expansion of the matrix with the increasing temperature, namely Rc is increased. Hence the AC conductivity decreases below 116 ℃. Above 116 ℃, the AC conductivity increases with the increasing temperature, because the charge carriers can drift over larger distances at higher temperature. It is evident that the frequency dependence of AC conductivity became pronounced with the increasing temperature, especially above 116 ℃. The reason is that the component of contact capacitors (Cc), which has a strong dependence on frequency, increased with the increasing temperature.

Figure III-6 shows the logarithm plots of the real part of complex permittivity ε' (dielectric permittivity) and the imaginary part of complex permittivity ε'' (dielectric loss) against frequency. In Figure III-6a, it is seen that the curves also can be distinguished between the two groups, especially at frequency higher than 10^3 Hz. The dielectric permittivity ε' of the different temperatures is nearly same value in the whole frequency range when the temperature is lower than 116 ℃. Both ε' and ε'' increase with the decrease of frequency at all temperature levels. Such phenomenon is more pronounced at lower frequencies (below 10^3Hz). The increment in permittivity with the decrease of frequency reveals that the system exhibits the interfacial polarization at low frequency. As reported by Soares et al[37], the strong low frequency

dispersion for ε' and no loss peak for ε'' are characteristics of charged carrier systems.

It is of interest to observe that the frequency dependence of logarithm plots of ε'' appears as straight lines at lower frequencies in the given temperature range as shown in Figure III-6b. The loss factor (ε''_{obs}) may be regarded as the contribution of three distinct effects. That is [38]:

$$\varepsilon''_{obs} = \varepsilon''_{dc} + \varepsilon''_{MW} + \varepsilon''_{D} \tag{III-7}$$

where ε''_{dc} is due to DC conductance, ε''_{MW} is due to interfacial polarization, and ε''_{D} is the usual dipole orientation or Debye loss factor.
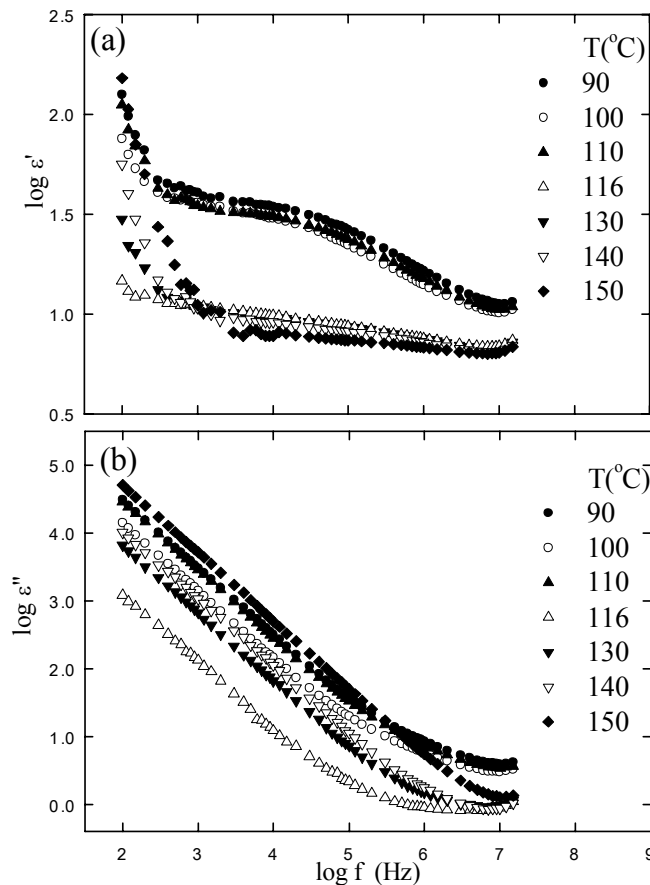

Figure III -6.   Logarithmic plots of complex permittivity versus frequency with different temperature: (a) permittivity and (b) loss factor

By considering the composites as parallel resistor-capacitor circuit system[39], some

mathematical equations have been developed to distinguish between loss (ε''_{dc}) arising from a DC conductivity process and from other sources of different processes. The loss factor due to DC conductance (ε''_{dc}) is given by Eq. (III-8):

$$\varepsilon''_{dc} = \frac{1.8 \times 10^{12}}{f} G_{spec} \tag{III-8}$$

where G_{spec} is the specific conductivity ($\Omega^{-1}cm^{-1}$) of the sample.

The loss factor due to the Maxwell–Wagner–Sillars (MWS) relaxation or interfacial polarization (ε''_{MW}) is given by Eq. III-9[40]

$$\varepsilon''_{MW} = \varepsilon_{\infty}(1 + \frac{K}{1 + \omega^2 \tau^2}) \tag{III-9}$$

where ε_{∞} and K are constants calculated considering two different dielectric permittivity of the sample at the interfaces and τ is the relaxation time of the interfacial polarization. By expressing the two above equations in logarithm form and plotting log (ε''_{dc}) and log (ε''_{MW}) vs the log(f) , two different curves will be obtained. The log (ε''_{dc}) vs the log (f) represents a straight line and the log (ε''_{MW}) vs the log (f) represents a sigmoidal curve. The increase of the loss factor (ε''_{obs}) with the decreasing of frequency in Figure III-6b suggests that DC conductivity process (namely, the current through an internal contact resistor Rc in the circuit model) is more significant than interfacial polarization (namely, the current through a contact capacitor Cc in the circuit model) at the temperature lower than 116 ºC, and the interfacial polarization becomes pronounced at the temperature higher than 116 ºC, since the interfacial polarization equation does not follow a linear behavior at higher frequencies. However, the interfacial polarization in Figure III-6b is not so obvious because it is obscured by the conductivity.

To facilitate the understanding of the influence of the temperature on the AC conductivity and permittivity, the logarithmic plots of AC conductivity σ_{AC} and

29

permittivity ε' vs temperature are shown in Figure III-7. A sharp decrease of AC conductivity σ_{AC} and permittivity ε' was observed at the temperature close to 116 ºC. Compared to DC conductivity (f = 0 Hz), the PTC intensity (= σ_P / σ_{RT} defined as the ratio of peak conductivity σ_P to the room temperature conductivity σ_{RT}) was not so huge and decreased with the increasing frequency. Moreover, NTC phenomenon appeared above 116 ºC can be observed in AC conductivity since the current through a contact capacitor C_c increased, and the charge carriers could drift over larger distances at higher temperature.
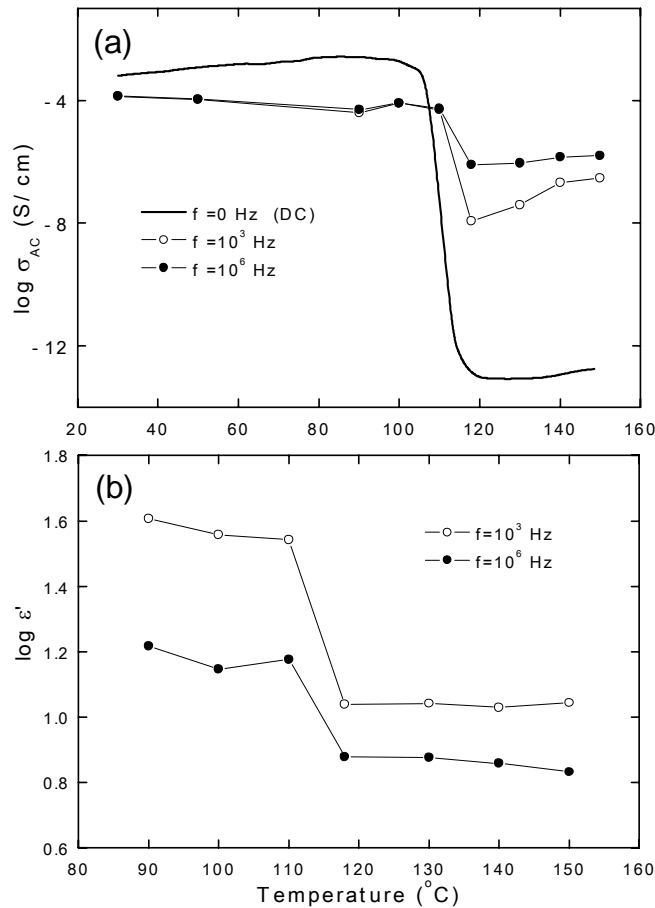

Figure III - 7. Logarithmic plots of (a) AC conductivity σ_{AC} and (b) permittivity ε' versus temperatures

Generally in systems with a conductive component, interfacial relaxation is obscured by conductivity and the dielectric permittivity may be high at low frequencies. To overcome this difficulty in evaluating interfacial polarization, it has been decided to use the electric modulus formalism. It has also been used to study the conductivity

relaxation behaviors of polymer[41].   An advantage of adopting the electric modulus to interpret bulk relaxation properties is that variations in the large values of permittivity and conductivity at low frequencies are minimized. In this way the familiar difficulties caused by electrode nature and contact, space charge injection phenomena and absorbed impurity conduction effects, which appear to obscure relaxation in the permittivity presentation, can be resolved or ignored[42].
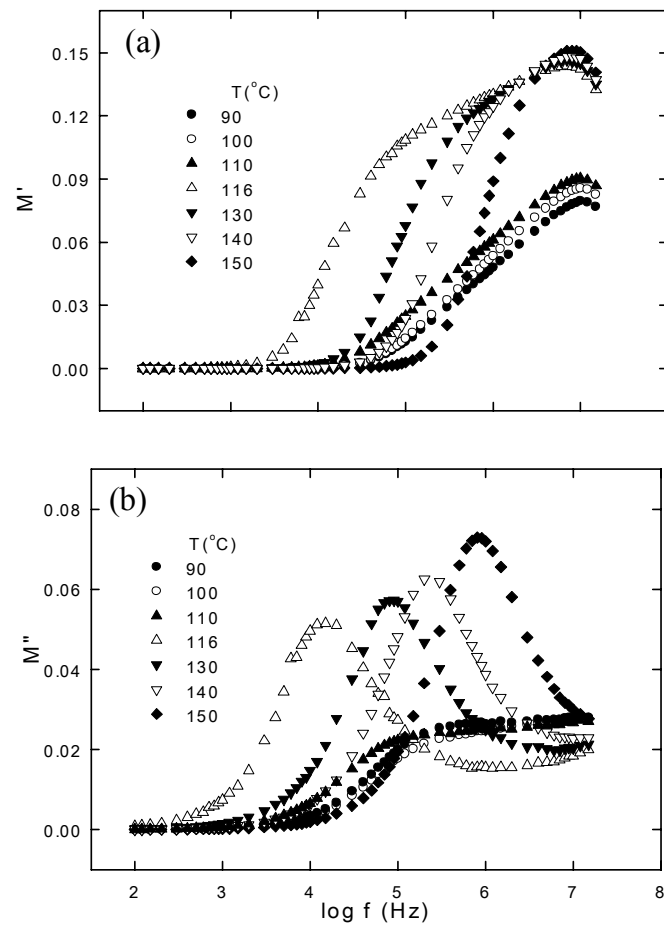

Figure III - 8. The electrical modulus versus log f with different temperature:(a) the real part and (b) the imaginary part

Our data can be analyzed by using the formalism of electric modulus introduced by MćCrum *et al.*[39].   The isothermal dependence of M'' with the frequency shown in Figure III-8 exhibits a loss peak, which is attributed to MWS effect, at temperature higher than 116 °C and these relaxation peaks move towards higher frequencies as temperature increases. At the lower temperatures than 116 °C, however, the composite exhibits no loss peak, indicating clearly that there is no relaxation processes. It also can

be explained by our circuit model. The current through an internal contact resistor R_c is principal when temperature is lower than 116 ºC, while the current through a contact capacitor C_c becomes principal when temperature is higher than 116 ºC.
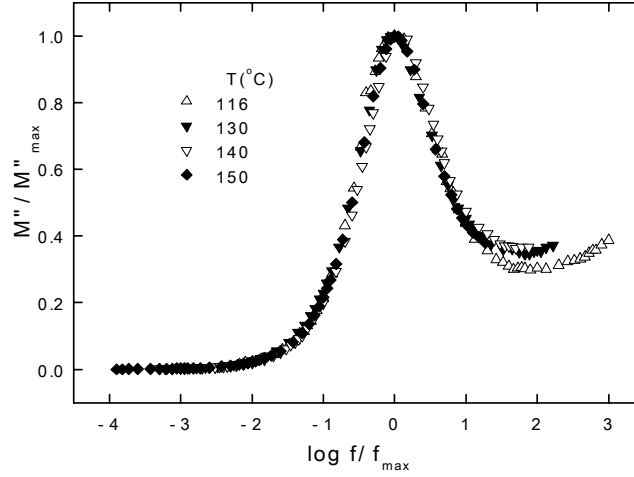

Figure III -9.   Normalized plots of of M"/M"$_{max}$ vs log(f/fmax) of the composites with different temperature

Figure III-9 shows the reduced plots of M'/M''_{max} vs log(f/fmax) at different temperatures that provide additional information regarding the molecular heterogeneity of the polymers. These plots show that the distributions of relaxation times are nearly the same over the temperature ranging from 116 ºC to 150 ºC.   The asymmetric shape of the plots indicates that the dielectric relaxation process deviates from the pure Debye behavior, and there exists a asymmetric distribution of relaxation times.

To pursue further analysis of the experimental results, the obtained data were fitted according to the Cole-Davidson approach, which anticipates an asymmetric distribution of relaxation times.   In the electric modulus formalism, the Cole-Davidson equations have the following form[42]

$$M' = \frac{M_\infty M_s [M_s + (M_\infty - M_s)(\cos\phi)^\gamma \cos\gamma\phi]}{M_s^2 + (M_\infty - M_s)(\cos\phi)^\gamma [2M_s \cos\gamma\phi + (M_\infty - M_s)(\cos\phi)^\gamma]}$$

(III-10)

$$M'' = \frac{M_\infty M_s (M_\infty - M_s)(\cos\phi)^\gamma \sin\gamma\phi}{M_s^2 + (M_\infty - M_s)(\cos\phi)^\gamma [2M_s \cos\gamma\phi + (M_\infty - M_s)(\cos\phi)^\gamma]}$$

where M_s is the value of M' when $\omega \to 0$ and M_∞ is the value of M' when

$\omega \to \infty$, $0 \le \gamma \le 1$, $tg\phi = \omega\tau$, $\omega_{max}\tau = tg(\dfrac{1}{\gamma+1}\dfrac{\pi}{2})$
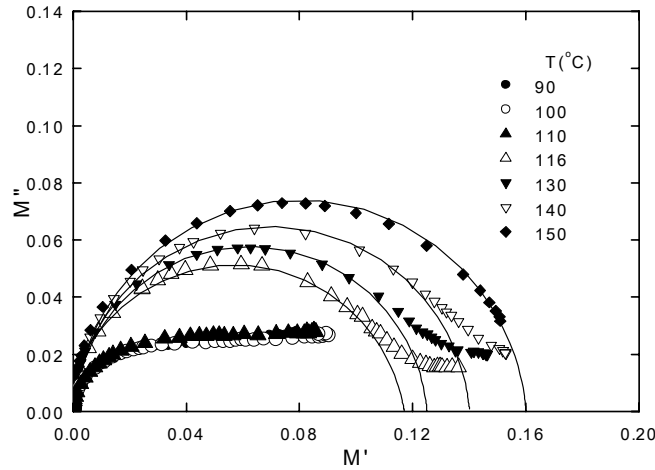

Figure III - 10. Cole-Cole plots of the electrical modulus of composites, the solid curves are produced by best-fitting experimental points to the Cole-Davidson approach

The complex plane diagram of the electric modulus illustrated in Figure III-10 displays single arcs at the temperatures higher than 116 ºC, which proves the existence of the interfacial or MWS relaxation process described above. Furthermore, it can be regarded as the transition from resistive conduction through the conduction networks of carbon fibers (namely, through the Rc) to the capacitance conduction through the capacitors (namely, through the Cc) in the matrix. This also indicates that the mechanism of PTC phenomenon is attributed to the conduction transition as a result of matrix thermal expansion. In Figure III-10 the produced fitting curves are compared with experimental data from specimens with varying temperature. The suppressed semi-circles in the Cole–Cole diagram correspond to the relaxation processes for each of the specimens.

It is worth noting that at low frequencies the fitted curves are in good agreement with the experimental data. The coincidence of the beginning of the semicircles with the origin of the graph provides a clear indication that no other relaxation process is present, at lower frequencies, in the studied systems. On the other hand, the variation of the

semicircles' radius is the result of the changing temperature. The parameters evaluated from the fitting procedure are listed in Table III-1. The exponent γ is a measure of the width of the distribution of relaxation times and $\gamma = 1$ corresponds to a single relaxation time process or a pure Debye type relaxation. The obtained values of the parameter γ are all higher than 0.9 indicating a rather narrow distribution of relaxation times.

Table III-1 Parameters used/evaluated for the Davidson-Cole function

Temperature(°C)	M_s	M_∞	τ_m (s)	γ	E_m (eV)
116	9.8×10^{-6}	0.117	1.112×10^{-5}	0.942	
130	3.2×10^{-4}	0.125	1.861×10^{-6}	0.937	1.661
140	3.6×10^{-7}	0.140	8.190×10^{-7}	0.964	
150	5.8×10^{-8}	0.159	2.069×10^{-7}	0.951	

Therefore, the activation energy of these relaxation processes can be estimated according to

$$\tau_m = \tau_0 \exp(\frac{E_m}{kT}) \qquad \text{(III-11)}$$

where E_m is the activation energy of the relaxation process, k is the Boltzmann constant ($k = 1.381 \times 10^{-23} J/K$) and T is the absolute temperature. Figure III-11 shows the linear relationship between $\ln \tau_m$ against the reciprocal of T. The value of the activation energies was calculated via a linear regression and by employing Eq. III-11.

Another interesting phenomenon for the composites is the time dependence of electrical conductivity. The sample was kept at 90°C for different time from 2 minutes to 25 days. The AC conductivity of the composites as a function of the keeping time is shown in Figure III-12. The logarithm plots of AC conductivity increase rapidly in the initial stage of the heat treatment, and then keep constant, which is similar to the AC

conductivity of the composites at room temperature (about $10^{-3.87}$ S/cm). Such behavior may be explained by the reconnection of filler clusters that were previous separated by matrix expansion. According to Sumita *et al.*[43], the filled conductive polymer composites are thermodynamically non-equilibrium system, in which conductive network formation is dependent on temperature and time, and a concept named as dynamic percolation has been proposed.
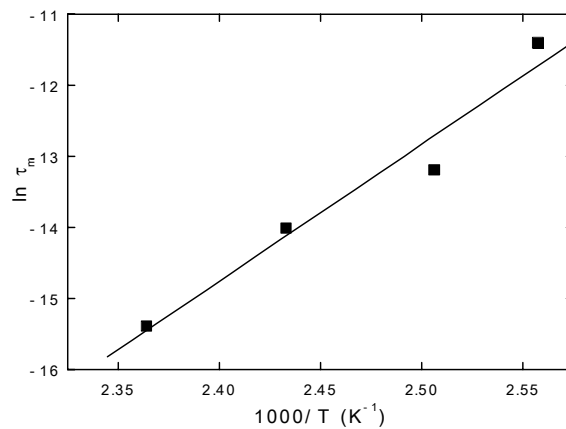

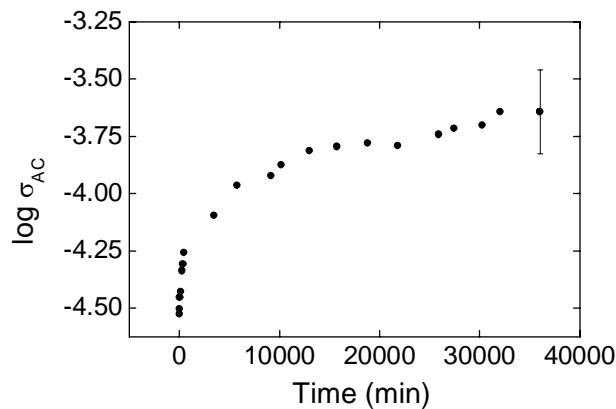FigureIII -11. Arrhenius plots of relaxation times versus 1/T and the respective linear fits of the composites.

Figure III -12. Logarithmic plots of AC conductivity versus time keeping at 90 ℃ and 1000Hz.

With increasing time, the new conducting network is formed as a result of the shift of carbon fibers. The experimental evidence can be found in the Figure III-13, in which the M' and M'' are given as a function of frequency for the sample kept at 90℃. The shift of M' and M'' to higher frequency with the increasing heat treat time provides the experimental evidence of dynamic percolation. This shifting also indicates that the

resistance, which is the sum of the small resistors made of carbon fillers in the matrix, becomes more significant than capacitance conductivity attributed to capacitors made of the gaps between carbon fibers.
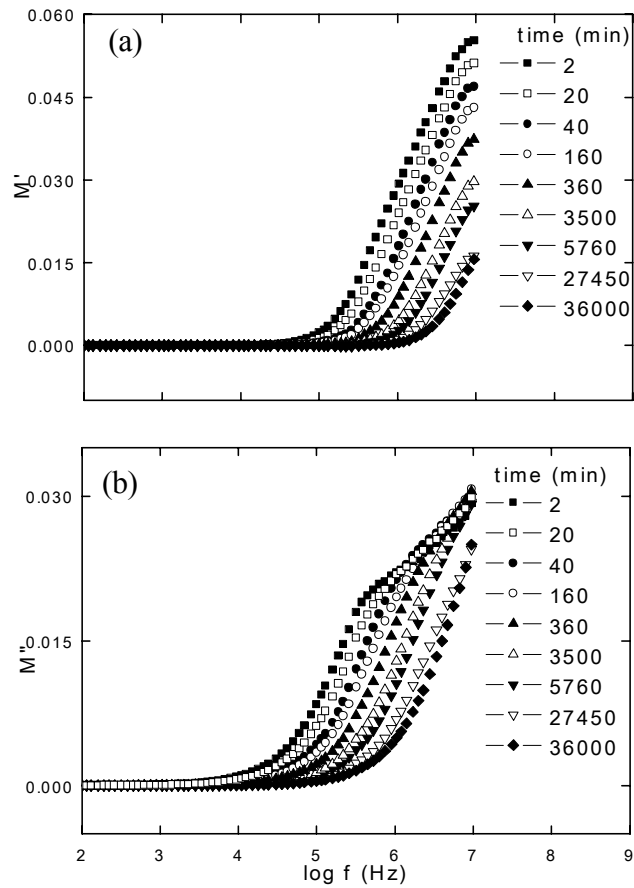

Figure III -13. The electrical modulus versus log f with time keeping at 90ºC: (a) the real part and (b) the imaginary part

IV. Electric and Mechanical Properties of Iodine-Doped Polymer-CNT Composites

As technology and science advance, there is an increasing demand for the development of materials with good mechanical and electrical properties. Many efforts have been made to produce carbon nanotubes reinforced polymer composite[1-4] and to improve the properties of polymer[5-8]. The elongation of polymer film has been studied [9-10] in terms of promotion of its mechanical properties by improving degree of molecular chain orientation. On the other hand, iodine doping has been studied to improve the electrical conductivity in several polymers[11-15]. Doped polypropylene (PP) with iodine has been observed to increase its conductivity due to the formation of charge transfer complex[15]. Iodine doping of the ion-implanted polyethylene resulted in the immediate and provided drastic increase of the sheet conductivity by 3-4 orders[16]. Furthermore, carbon nanotubes can be doped by suitable donor or acceptor dopants[17-19] and the doping facilitates the charge transfer between dopants and tubes.

We have prepared the composite films of ultrahigh molecular weight polyethylene (UHMWPE) with multiwalled carbon nanotubes (MWNTs) by gelation/crystallization [20]. The resultant MWNTs-UHMWPE film could be elongated up over 100-fold. The co-orientation of UHMWPE and MWNTs assured the elongated film possessing high mechanical properties. However, there are no reports, to the best of our knowledge, on the effect of doping on the electrical and mechanical properties of MWNTs and PE composites. In order to improve the electrical conductivity of the composites, the iodine-doping was carried out for the highly oriented MWNTs-UHMWPE films in this research. With this significant lack of information, this research sheds some light onto this future-promised but presently limited-data area. Structure and property changes induced by iodine doping have been investigated by Raman scattering and differential scanning calorimetry techniques and measurements of mechanical and electrical properties were carried out.

The MWNTs named Hyperion Graphite Fibrils were produced by Hyperion with a diameter (D) of 10-20 nm, a length (L) of 10 ~ 20 μm, and an aspect ratio (L/D) of (1 ~ 2) x 10^3. The BET surface area was 250 m^2/g, and the DBP adsorption was 400-500 cm^3/100 g. The density was 2.0 g/cm^3.

The drawn films were set in a desiccator containing iodine crystal. After being degassed, the desiccator was heated to 80°C at the heating rate of 5 °C/min and saturated by iodine vapor. The samples were put in the saturated iodine vapor at 80°C for 6h. After then, the samples were picked out and washed by ethanol till the solvent was colorless, and then vacuum-dried for 24h. The electrical conductivity was measured soon after vacuum-drying.
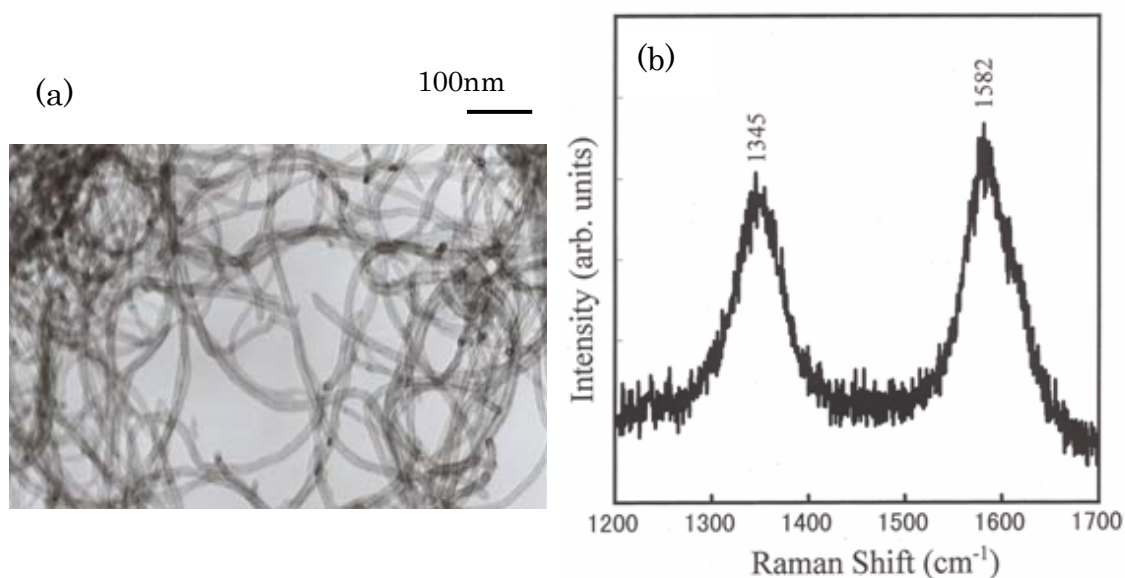
Figure IV-1. (a) TEM image and (b) Raman spectrum of MWNTs

Figure IV-1 shows a transmission electron microscope (TEM) image and the Raman spectrum observed with an excitation laser wavelength of 488 nm. Image (a) indicated that the MWNTs possessed high purity and uniform diameter distribution. In Raman spectrum (b), however, the peak of the Raman-allowed phonon mode, at 1582 cm^{-1}, was not very sharp, and the intensity of the peak at 1345 cm^{-1} was high which appeared

through the disorder-induced phonon mode[21]. It indicated the present MWNTs had a low degree of graphitization.
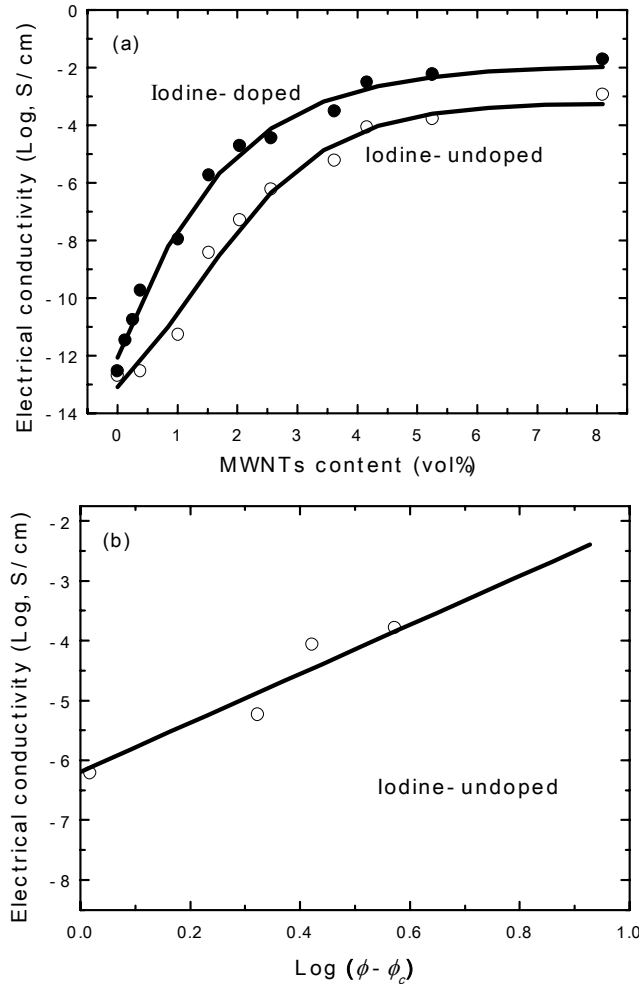

Figure IV-2. (a) Electrical conductivity versus volume fraction of MWNTs; (b) Log-log plot of the conductivity against Φ-Φ_c with Φ_c=1.52 vol% according to Eq. IV-1

Figure IV-2 shows the electrical conductivity of the MWNTs-UHMWPE films as a function of the MWNT content, which were prepared by drawing the original films to 50-fold. The value of the electrical conductivity of the drawn films increased 9 orders of magnitude from 10^{-13} S/cm to 10^{-4} S/cm with increasing the content of MWNTs, and tended to level off around 4.16 vol% MWNTs. This indicates a typical percolation transition behavior. In Figure IV-2(a), it is clearly seen that the conductivity of iodine-doped MWNTs-UHMWPE films was improved one to four orders of magnitude

compared with the undoped films, but the trend of the conductivity versus the volume fraction of MWNTs was hardly affected by iodine doping. Further, it is found that the conductivity of neat UHMWPE did not change by iodine doping.   This tendency is different from the result by Lewis et al. reported for undrawn low molecular weight polyethylene films[16].

According to classical percolation theory[22], the conductivity of composite film as a function of conductive filler can be described by a scaling law of the form:

$$\sigma = \sigma_0(\Phi - \Phi_c)^t \qquad\qquad\qquad (IV\text{-}1)$$

where Φ is the volume fraction of the filler, Φ_c is the percolation threshold, σ_0 is the conductivity of the filler, and t (>0) is the universal critical exponent characterizing the relationship between σ and Φ. This equation is valid when $\Phi > \Phi_c$ and ($\Phi - \Phi_c$) is small. As the volume fraction increases beyond the percolation threshold, the conductivity increases sharply as conductive paths begin to form. For the present drawn films, the conductivity of pristine films is plotted logarithmically as shown in Figure IV-2(b). Fitting the observed data according to Eq. IV-1 gives the parameters Φ_c=1.52 vol% (3wt%) and t=4.09. Many authors had verified the scaling law on CNT-polymer composite[23-25]. Various values between 8 wt% [23] and 0.0025 wt% [25] had been reported as the percolation threshold for the CNTs-filled polymer composite. Many factors such as distribution of CNTs, CNTs-matrix interaction and processing technique were thought to influence the percolation threshold significantly. On the other hand, the t value obtained in this research is higher than very high t values, 3.1[26] and 3.3[27], reported for carbon fiber[26]. The reason may be the high aspect ratio of the MWNTs as described in Experimental, which is helpful to develop the conductive paths due to easy formation of cross-linking structure.

To better understand an increase in the conductivity and study the mechanism, the Raman spectra were measured after washing the composites by ethanol. Figure IV-3 shows the spectra of iodine measured for the elongated composite films with 1.52 vol% MWNTs, namely, (a)-pristine and (b)-the iodine-doped MWNTs-UHMWPE film stored

in desiccator for two months. As shown in Figure IV-3(b), the strong and broad peak at 175 cm^{-1} and a very weak peak at 110 cm^{-1} were observed. These peaks were assigned, respectively, to the I_5^- and I_3^- polyiodine chains, similarly to the cases of the iodine-doped single-wall carbon nanotubes[28]. Raman peak at 215 cm^{-1}, which is due to the existence of neutral or dissociative molecular iodine (I_2^0)[29], is not observed. This indicates that no excessive iodine existed in the sample after being washed with ethanol and vacuum-drying. Considering the low intensity of I_3^-, the increase in the electrical conductivity is assumed mainly due to the I_5^- which acts as the charge carriers to form the charge transfer complex. In spite of the washing, the existence of the I_5^- and I_3^- peaks is interesting phenomenon different from the result by Michel et al.[30] This indicates strong interaction between iodine and networks of MWNTs and UHMWPE chains. The quantitative estimation for doping concentration, however, still remains unresolved problem.
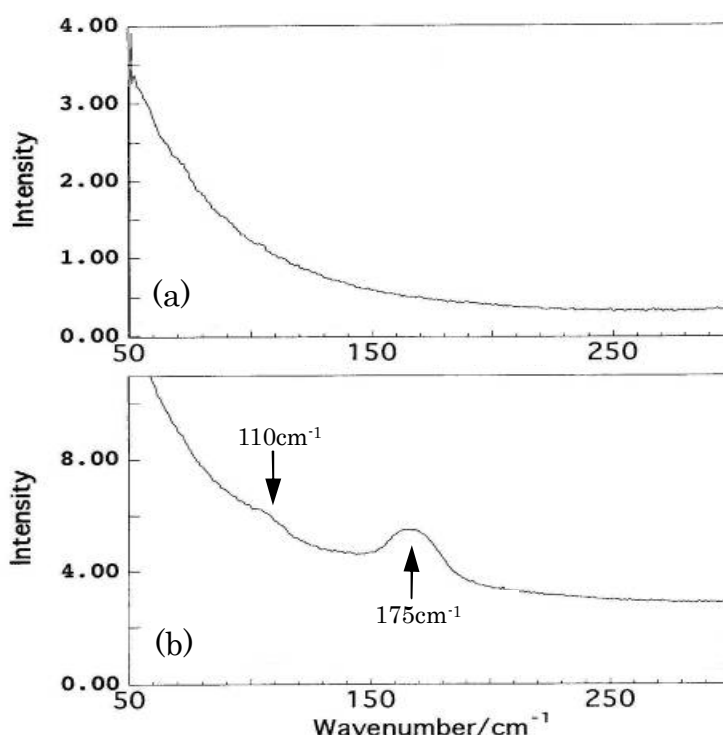

Figure IV-3. Raman spectra of the iodine-doped composite films with 1.52 vol% MWNTs using a 514.5nm excitation: (a) pristine and (b) 2 months after doping
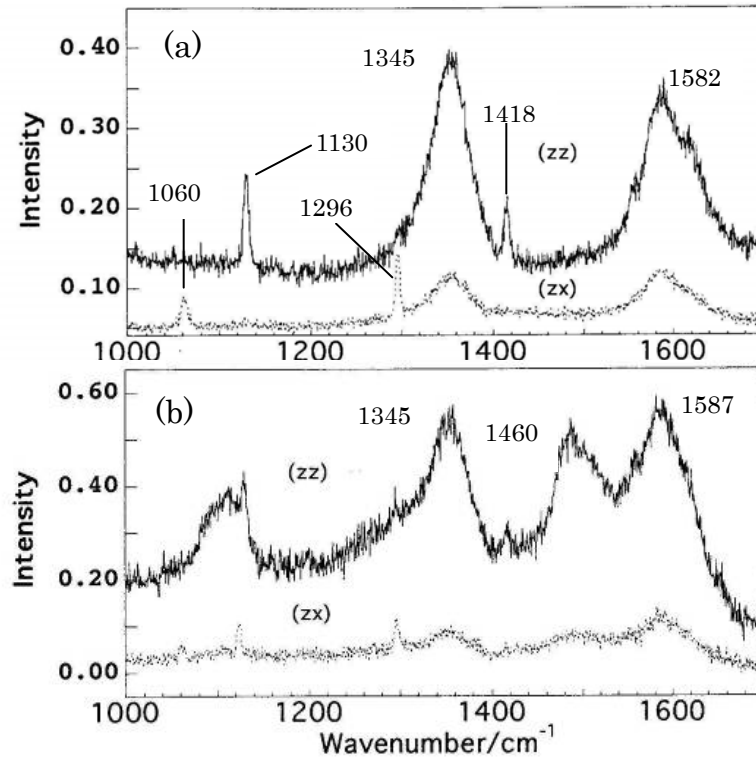
Figure IV-4. Raman spectra of the composite films with 1.52 vol% MWNTs doped iodine measured using a 514.5nm excitation: (a) pristine and (b) 2 months after doping

In Figure IV-4, Raman spectra of (a)-pristine and (b)-the iodine-doped MWNTs-UHMWPE film kept in desiccator for two months are shown, where the (ZZ) and (ZX) polarization components are presented. In this figure, the Z axis is the drawn axis and the X axis is perpendicular to Z axis. As for the D-mode (1345cm^{-1}) and G-mode (1582cm^{-1}) of MWNTs, the intensity of (ZX) component is much lower than that of the (ZZ) component, suggesting that most of MWNTs in the films are oriented along the chain axis. For the pristine sample, the peaks at 1060, 1296, 1130 and 1418 cm^{-1} correspond to polyethylene. The band assignments are listed in Table IV-1[31]. When the films were doped with iodine, the peak at 1130 cm^{-1} due to the C-C stretching mode became broader, and a new peak appeared at about 1460 cm^{-1}, being attributed to the CH$_2$ bending mode belonging to the amorphous phase. Iodine, a highly electronegation, could interact with the UHMWPE lattice and produce the distortions

and stresses within the crystallites, thereby led to structural modifications. This phenomenon was also found in other polymers, such as PP[32] and low density polyethylene (LDPE)[33].

Table IV-1. Assignments of the Raman bands of polyethylene

frequency, cm^{-1}	phase	mode	symmetry
1060	C (A)	υ_{as}(C-C)	$B_{2g}+B_{3g}$
1080	A	υ(C-C)	
1130	C (A)	υ_s(C-C)	A_g+B_{1g}
1170	C (A)	ρ(CH$_2$)	A_g+B_{1g}
1296	C	τ(CH$_2$)	$B_{2g}+B_{3g}$
1310	A		
1370	C	ω(CH$_2$)	$B_{2g}+B_{3g}$
1418	C	δ(CH$_2$)	A_g
1440	A	Fermi resonance +	$B_{1g}+A_g$?
1460	A	Overtones?	A_g+B_{1g}?

(Note: C, crystalline; A, amorphous; υ, stretching (s, symmetric; as, asymmetric); ρ, rocking; δ, bending; τ, twisting; ω, wagging)

The peaks at 1345 cm^{-1} and 1582 cm^{-1} are assigned to the D-mode and G-mode of MWNTs (shown in Figure 1), respectively. Comparing Figure 4(a) and (b), it is found that G-mode up-shifted 5 cm^{-1} after iodine doping. This result is in agreement with the study by Cambedouzou et al[34]. The outer tube vibrations are affected by the iodine doping. According to the reports by Michel et al[30] and Zhou et al[17], the adsorption of iodine occurs on the surface of MWNTs. Therefore, the content of MWNTs and the crystallinity of UHMWPE could influence the concentration of doped iodine. It is plausible that the enhancement degree of the conductivity is different, as shown in Figure IV-2.
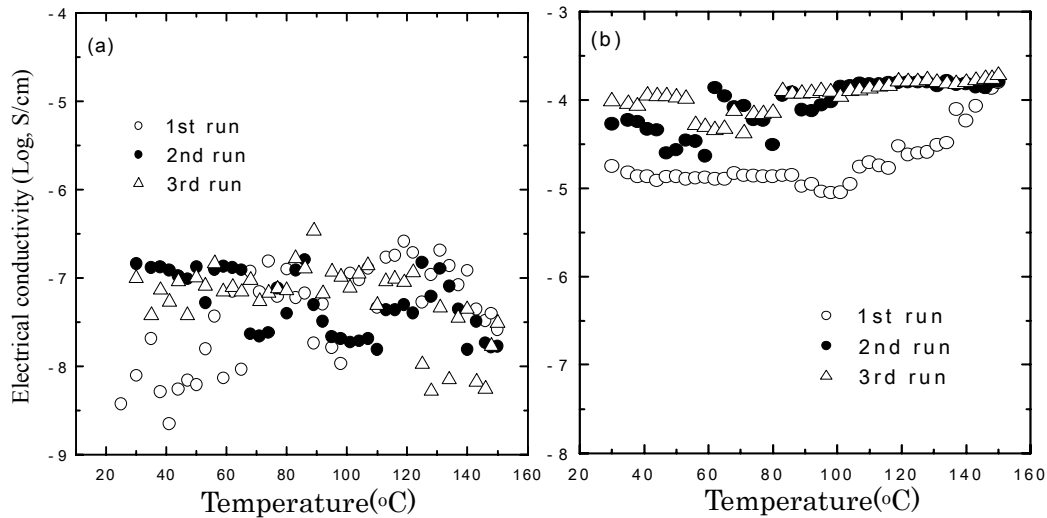
Figure IV-5. Electrical conductivity for the films with 1.52 vol% MWNTs during 3 heating cycles: (a) pristine, (b) iodine-doped

The temperature dependence of the electrical conductivity is investigated for the pristine and doped MWNTs-UHMWPE films drawn by 50-fold. The results for three heating cycles as the first (1st), second (2nd) and third (3rd) run in the temperature range from 25 to $150^{o}C$ are shown in Figures IV-5 and 6 for 1.52 and 4.16 vol% MWNTs, respectively. The repeated heat treatments were done at a constant length. For the films with 1.52 vol% MWNTs in Figure IV-5, the electrical conductivity of the pristine film was irregular for three cycles, indicating that the charge transfer was not smooth at the percolation threshold Φ_c. In this case, the content of MWNTs was the key for the formation of conductive network. It is thought that the thermally induced hopping transport between disconnected (or weakly connected) parts of the network is unstable. After iodine doping, the conductivity became regular. The I_5^-, as charge carrier, can be taken as bridge for the adjacent or nearby MWNTs. For the first heating run, the conductivity suddenly increased near the melting point of UHMWPE. In the second and third runs, the conductivity was slightly higher than that of the first run. Furthermore, comparing with the pristine film, the iodine doped film shows that the stability against temperature is promoted for all the three heating-runs. Beyond the

44

fourth run, the route of the temperature dependence is confirmed to be similar to the third run route, which indicates more stable electrical properties by heating treatment.
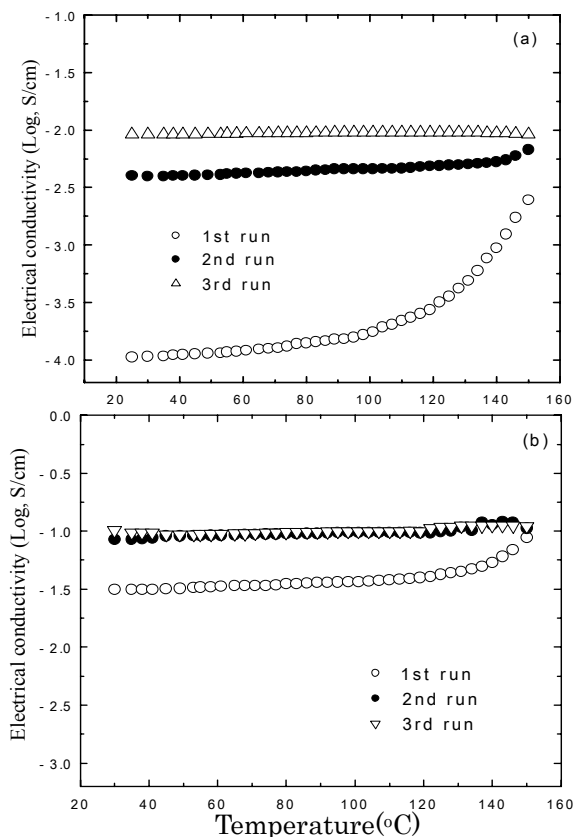
Figure IV-6. Electrical conductivity for the films with 4.16 vol% MWNTs during 3 heating cycles: (a) pristine, (b) iodine-doped

For the films with 4.16 vol% MWNTs ensuring enough conductive paths, the conductivity of the pristine film increased slowly from 25°C to 150°C as shown in Figure 6(a). When the temperature was over 120°C in the first run, there was also a sudden increase in the conductivity. But, for the second run, the conductivity was maintained constantly during the heating process up to 130°C and tended to increase slightly at further high temperature. Accordingly, it is of interest to consider that the conductivity increases by heat treatment up to 150°C. The conductivity of the pristine film obviously increased with temperature and the conductivity increased by an increase in heating cycles. According to the previous works[35-36], the scanning electron microscopy (SEM) observations revealed that the MWNTs within the matrix of the

original film (dry gel film) prepared in decalin were covered by UHMWPE, and their average diameters became much thicker than the original diameters of the MWNTs, indicating that most of the UHMWPE chains crystallized on the MWNT surface and acted as nuclear growth of UHMWPE under gelation process. However, when the original film was heated beyond the melting point of UHMWPE, the most of melted UHMWPE chains did not crystallized on the MWNT surface. SEM observation provided the dispersion of bare MWNTs in the UHMWPE matrix. The oriented crystallization for UHMWPE chains by the elongation of the original film at 135~140°C did not occur mostly on the surface of MWNTs. Accordingly, the conductivity (10^{-4} S/cm) of the drawn film with 4.16vol% MWNTs before the first heating run shown in Figure IV-6 was confirmed to be much higher than conductivity (10^{-8} S/cm) [20, 36] of undrawn films with the same MWNT content. The increase in conductivity by an increase in heating cycles is probably thought to be due to the perfect melting of residual trace of UHMWPE on the surface of some of MWNTs. Namely, the increase in conductivity of the pristine film with increasing temperature is attributed to an increase of mutual contact possibility of MWNTs.

As shown in Figure IV-6(b), the conductivity of the iodine-doped film is higher than that of the pristine film. The Raman spectra concerning the I_5^- shows the same profiles as Figure 3 for the films heat-treated up to 150°C. No weight loss was also confirmed by thermogravimetric analysis[17]. This indicates that the I_5^- localized on the outer layers of bare MWNTs and/or UHMWPE chains can be obviously maintained as charge transfer complex after the heat-treatment and played an important role to ensure good electrical conductivity of the iodine-doped system, because of an increase in charge carriers linked to the MWNTs. Namely, the I_5^- provided additional charge carriers to the UHMWPE-MWNT system and could be taken as bridge for the adjacent or nearly MWNTs.

Here it may be noted that the thermal expansion of UHMWPE at temperatures close to its melting point is not considerable enough to cause the separation of the contacted

MWNTs, so the conductive paths for charge transportation are maintained. Namely, the conductivity under the second and third runs was extraordinarily stable. The conductivity for the MWNTs-UHMWPE composite in the second heating cycle showed almost the constant values. This indicates that the cross-linking between flexible MWNTs[20] becomes tighter than the thermal expansion of UHMWPE after the first heating run. Accordingly, the thermal behavior of MWNTs-UHMWPE composites is different from that of carbon fiber-polyethylene composites taking positive thermal coefficient (PTC) effect[27].

Table IV-2. Change of crystallinity X_C (%) of UHMWPE within the composite films with non-doping and doping at different heating run

MWNTs content (vol%)	Before 1st run		After 1st run		After 2nd run	
	Non-doping	Doping	Non-doping	Doing	Non-doping	Doping
1.52	97.9	95.7	57.4	50.9	55.1	49.4
4.16	76.7	60.6	47.0	35.2	47.9	36.5

Thermal property of the doped films drawn up to 50-fold was studied by DSC analysis. The crystallinities of the pristine and doped films during three heating runs were calculated and listed in Table IV-2, where the crystallinity was calculated as the ratio of the observed Δh to Δh_f of a 100% crystalline polyethylene (245.3J/g)[37]. From Table IV-2, it can be seen that the crystallinity before the first run is higher than those after the first and second heating runs. The values after the second run tend to be almost the same after the first run. In addition, the crystallinity of the pristine film (before the first heating run) with MWNTs contents less than 1.52 vol% was nearly equal to 98%, indicating the remarkable orientated crystallization of UHMWPE. However, the oriented MWNTs beyond the percolation threshold (1.52 vol%) obviously hampered the orientated crystallization and an increase in crystallinity was quite less pronounced with increasing MWNT content. Furthermore, the crystallinity of the doped films was lower

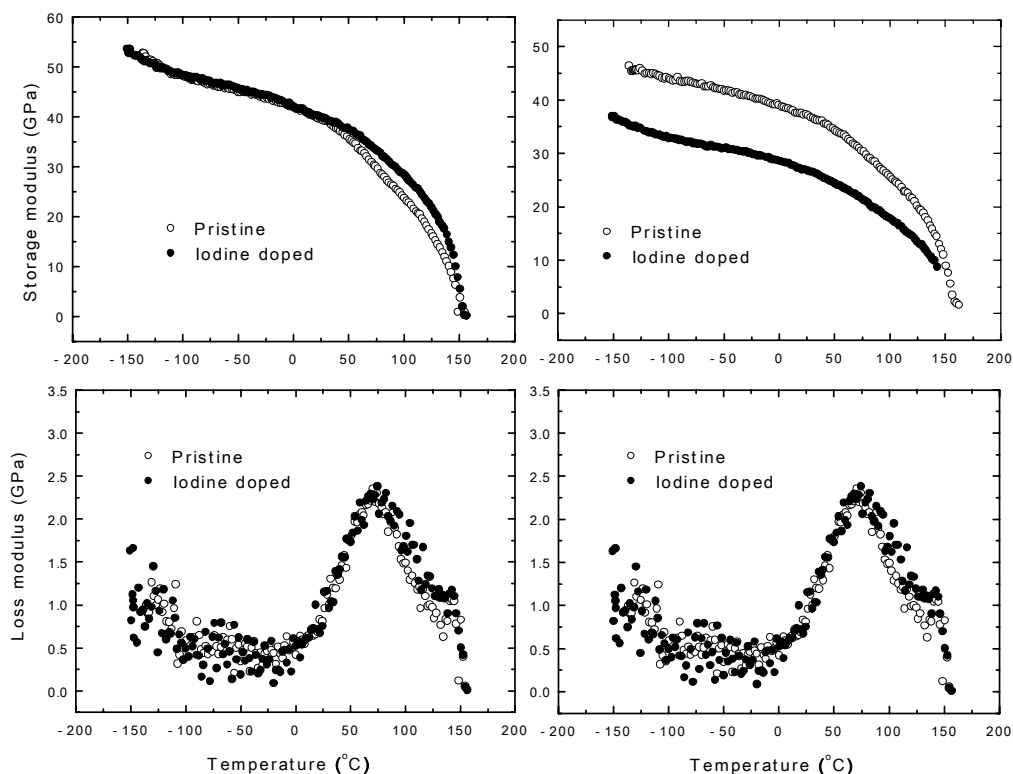than that of the pristine films. This behavior was in agreement with the Raman analysis (Figure IV-4).

Figure IV-7. Temperature dependence of storage and loss moduli of composite films at drawn ratio of 50-fold: (a) with 1.52 vol% MWNTs; (b) with 4.16 vol% MWNTs

Figure IV-7 (a) and (b) shows the temperature dependence of the storage modulus ($E^{'}$) and loss modulus ($E^{''}$) measured for the pristine and doped MWNTs-UHMWPE films with 1.52 vol% and 4.16 vol% MWNTs, respectively. The storage modulus of the film with 1.52 vol% MWNTs was slightly higher than that of the film with 4.16 vol% MWNTs indicating that an increase in MWNT networks hampered to promote oriented crystallization of UHMWPE chains. For the films containing 1.52 vol% MWNTs, no significant change in E' after iodine doping was confirmed, and E' reached 42GPa at 20°C, while the E' of doped film with 4.16% MWNTs was maintained ca. 25GPa at 20°C. From Table IV-2, it is known that by iodine-doping, the decrease of crystallinity of the film with 1.52vol% MWNTs was only 2.2% (from 97.9 to 95.7%), while that of

the film with 4.16vol% MWNTs was 16.7% (from 76.7 to 60.6%). Such drastic decrease could lead to the great decrease of the storage modulus by an increase in MWNT content. As for E'', the α-dispersion peak associated with crystal phase[38-40] showed no significant change indicating almost no change in activation energy of crystal dispersion. The β dispersion peak associated with amorphous phase[40] was not observed indicating no significant macro Brawnian motion of oriented amorphous chains[41] and then the drastic decrease of storage modulus did not occur around room temperature Anyway, the iodine-doping of the MWNTs-UHMWPE films provided good stability of electrical conductivity without drastic decrease of the mechanical properties. This indicated the iodine-doping for drawn MWNTs-UHMWPE film is potentially useful as the electronic or electrochemical devices which demand high mechanical properties.

Conclusion and Remarks

1) Under electric field, the orientation energy due to the permanent dipole is linearly dependent on electric field strength, while the energy due to the induced dipole depends upon the square of the field strength.   On the other hand, the orientation energy under the magnetic field is proportional to the square of the magnetic flux density B and the origin of the diamagnetism is the induced magnetization caused by the induced motion of electrons under the applied magnetic field. In comparison with the experimental (predicted) and theoretical results, it turned out that the effective magnetic orientation of CF axes was found to be significant to overcome the collision of neighbor CFs before the formation of stiff gels. Namely, it was evident that the orientational degree of CF axes sat the equilibrium state becomes lower and the period up to the equilibrium becomes longer with increasing viscosity of the solution.

2) Good PTC effect was achieved using LMWPE-UHMWPE-CF blends prepared by gelation/crystallization from dilute solution. The PTC effect exists in the wide fiber

content range. The maximal PTC effect, the intensity of which being about 9 orders of magnitude, was presented with a LMWPE/UHMWPE composition of 9/1 containing 23.5 vol% CF much higher than the percolation threshold value.

The elimination of the NTC effect and the improvement of reproducibility of electrical conductivity were found to be achieved by using a very high viscosity semicrystalline polymer as one of the composites such as UHMWPE. The origin of PTC phenomenon was due to the change of the distribution of the interparticle gap width between carbon fibers in the molten state of the polymers. The DSC results indicated that the carbon fibers have no significant influence on the morphology of polyethylene such as the crystallinity and the grain size.

3) Single parallel resistor-capacitor circuit model was used to study the AC electrical response of PTC composites consisting of UHMWPE/LMWPE matrix with randomly dispersed short carbon fibers. Similar to the DC electrical conductivity, PTC effect also can be observed in the AC electrical conductivity at a temperature close to 116 ºC because the conduction networks are broken. And NTC effect can also be observed because the component of contact capacitors has a strong dependence on frequency and temperature. Furthermore, the MWS relaxation found in the dielectric spectra of the composite systems indicates that the interfaces, which may be associated with melting polyethylene, were introduced between carbon fibers above 116 ºC. By employing the electric modulus formalism in the frequency ranging from 100 Hz to 10 MHz, the observed relaxations can be described by the Cole-Davidson distribution of relaxation times. The AC conductivity increases with increasing heat treat time as a result of reconnection of carbon fibers in the polymer matrix.

The present note (paper) of electrical relaxation phenomena for PTC effect offers not only the potential application of this material, but also insightful information concerning the molecular mobility, polarization and PTC mechanism. Although our results are limited for carbon fibers, the analysis may be also applicable to the new important engineering composite materials such as carbon nanotube composites.

4) The conductivity was improved for pristine and doped films with increasing MWNT content, because of an increase of mutual contact possibility of MWNTs. That is, the conductivity of film with 4.16 vol% MWNTs was much higher than that with 1.52 vol% MWNT. The conductivity increased by iodine-doping and this tendency was

more considerable by heat-treatment. Raman spectroscopy indicated that the doped iodine existed mainly as I_5^-, which formed the charge transfer complex. The I_5^- localized on the outer layers of bare MWNTs and/or UHMWPE chains played an important role to ensure further good electrical conductivity of the iodine-doped system. Namely, the I_5^- provided an increase in charge carriers linked to the MWNTs and could be taken as bridge for the adjacent or nearly MWNTs. The oriented crystallization of the films was less pronounced by an increase in MWNT content. Even so, the storage modulus of the iodine-doped film with 4.16 vol% MWNT was maintained ca. 25GPa at 20^oC. Accordingly, iodine-doping for drawn MWNTs-UHMWPE film was confirmed to be one of the useful techniques to develop high modulus and high conductive materials.

References

Chapter I

1) M. Narkis, A. Ram, F. Flashner, Polym. Eng. Sci., **18**, 649 (1978)

2) Y. Bin, C. Xu, Y. Agari, M. Matsuo, Colloid & Polym Sci., **277**, 452 (1999)

3) Y. Xi, H. Ishikawa, Y. Bin, M. Matsuo, Carbon, **42**, 1699 (2004)

4) Y. Bin, M. Kitanaka, D. Zhu, M. Matsuo, Macromolecules, **36**, 6213 (2003)

5) Y. Bin, Q. Chen, K. Tashiro, M. Matsuo, Physical Rev. B 77 035419 (2008)

Chapter II

1) C.T. O'Konski, K. Yoshioka, W.H. Orttung, J. Phys. Chem., 63, 1558 (1959)

2) M.J. Shah, J. Phys. Chem., **67**, 2215 (1963)

3) D.N. Holcomb, I. Tinoco, Jr., J. Phys. Chem., **67**, 2691 (1963)

4) F. Ozaki, T.Ogita, M. Matsuo, Macromolecules, **13**, 1187 (1981)

5) M. Matsuo, K.Kakei, Y. Nagaoka, F. Ozaki, M. Murai, T. Ogita,

J. Chem. Phys., **75**, 5911 (1981)

6) M. Matsuo, K. Kakei, F. Ozaki, T. Ogita, J. Chem. Phys., **76**, 3974 (1982)

7) M. Matsumoto, H. Watanabe, K. Yoshioka, J. Phys. Chem., **74**, 2182 (1970)

8) M. Matsuo, K.Kakei, Y. Nagaoka, J. Chem. Phys., **75**, 5925-5939 (1981)

9) E. Beaugnon and R. Tournier, Nature (London), **349**, 470 (1991).

10) M.V. Berry and A.K. Geim, Eur. J. Phys., **18**, 307 (1997).

11) V. Timbrell, J. Appl. Phys. **43**, 4839 (1972).

12) M.J. Matthews, M.S. Dresselhaus, G. Dresselhaus, M. Endo, Y. Nishimura, T. Hiraoka, N. Tamaki, Appl. Phys. Lett. **69**, 430 (1996).

13) M. Fujiwara, E. Oki, M. Hamada, Y. Tanimoto, I. Mukouda, and Y. Shimomura, J. Phys. Chem. A, **105**, 4383 (2001).

14) T. Kimura, H. Ago, M. Tobita, S. Ohshima, M. Kyotani, and M. Yumura, Adv. Mater., **14**, 1380 (2002).

15) M.J. Casavant, D.A. Walters, J.J. Schmidt, and R.E. Smalley, J. Appl. Phys. **93**, 2153 (2003).

16) J.E. Fischer, W. Zhou, J. Vavro, M.C. Llaguno, C. Guthy, R. Haggenmueller, M.J. Casavant, D.E. Walters, and R.E. Smalley, J. Appl. Phys., **93**, 2157 (2003).

17) T. Takahashi, K. Yonetake, K. Koyama, T. Kikuchi, Macromol. Rapid Commun., **24**, 763 (2003).

18) J. Sujiyama, H. Chanzy, and G. Maret, Macromolecules, **25**, 4232 (1992).

19) J.-F. Revol, L. Godbout, X.M. Dong, D.G. Gray, H. Chanzy, and G. Maret, Liq. Cryst., **16**, 127 (1994).

20) X.M. Dong and D.G. Gray, Langmuir, **11**, 3029 (1997).

21) T. Kimura, T. Kawai, and Y. Sakamoto, Polymer, **41**, 809 (2000).

22)T. Kimura and M. Yoshino, Langmuir, **21**, 4805 (2005).

23)T. Kimura, Polym. J. (Tokyo, Jpn.), **35**, 823 (2003).

24) R.W. Duke and D.B. Dupre', Macromolecules **7**, 374 (1974).

25) D.B. Dupre'and R.W. Duke J. Chem. Phys. **63**, 143 (1975).

26) Y. Bin, M. Kitanaka, D. Zhu, M. Matsuo   Macromolecules, 36 6213 (2003)

27) Y. Bin, M. Mine, A. Koganemaru, X. Jiang, and M. Matsuo, Polymer **47**, 1308 (2006).

28) S. Broersma, J. Chem. Phys. **32**, 1626 (1960).

29) R.J. Roe and W.R. Krigbaum, J. Chem. Phys. **40**, 2608 (1964).

30) W.R. Krigbaum and R.J. Roe, J. Chem. Phys. **41**, 737 (1964).

31) R.J. Roe, J. Appl. Phys. **36**, 202 (1965).

32) M. Matsuo, K. Hirota, K. Fujita, and H. Kawai, Macromolecules **11**, 1000 (1978).

33) M. Matsuo, F. Ozaki, H. Kurita, S. Sugawara, and T. Ogita, Macromolecules **13**, 1187 (1980).

34) T. Nakashima, C. Xu, Y. Bin, and M. Matsuo,

Polym. J. (Tokyo, Jpn.) **33**, 54 (2001).

35) Y. Bin, A. Koganemaru, T. Nakashima, and M. Matsuo,

Polym. J. (Tokyo, Jpn.), **37**, 192 (2005).

36) M. Matsuo, C. Sawatari, Y. Iwai, F. Ozaki, Macromolecules **23**, 3266 (1990).

37) Y. Bin, Y. Tanabe, C. Nakabayashi, H. Kurose, and M. Matsuo,

Polymer **42**, 1183 (2001).

38) M. Matsuo, Y. Bin, M. Nakano, Polymer **42**, 4687 (2001).

39) M. Matsuo, R. Sato, N. Yanagida, Y. Shimizu, Polymer, **33**, 1640 (1992).

40) M. Matsuo, R. Adachi, X. Jiang, and Y. Bin, Macromolecules **37**, 1324 (2004).

41) Y. Bin, K. Ooshi, K. Yoshida, T. Nakashima, M. Matsuo,

Polym. J. (Tokyo, Jpn.), **36**, 394 (2004).

Chapter III

1) Meyer J., *Polym Eng Sci.*, *13*: 462 (1973)

2) Meyer J., *Polym Eng Sci.*, *14*: 706 (1974)

3) Narkis M., Ram A., Flashner F., *Polym Eng Sci.*, *18*: 649 (1978)

4) Narkis M., Ram A., Stein Z., *Polym Eng Sci, 21*: 1049 (1981)

5) Narkis M., Vaxman A., *J Appl Polym Sci.*, *29*: 1639 (1984)

6) Tchoudakov R., Breuer O., Narkis M., Siegmann A., *Polym Eng Sci.*, *36*: 1336 (1996)

7) Xu C., Bin Y., Agari Y., Matsuo M., *Colloid Polym Sci.*, *276*: 669 (1998)

8) Bin Y., Xu C., Agari Y., Matsuo M., *Colloid Polym Sci.*, *277*: 452 (1999)

9) Bin Y., Xu C., Zhu D., Matsuo M., *Carbon*, *40*: 195 (2002)

10) Chekanov Y., Ohnogi R., Asai S., Sumita. M., *Polymer J., 30*: 381 (1998)

11) Vilcakova J., Saha P., Quadrat O., *Eur Polym J.*, *38*: 2343 (2002)

12) Tavman I.H., *J Appl Polym Sci* **1996**, *62*: 2161

13) Ohe K., Naito Y., *Jpn J Appl Phys* **1971**, *10*: 99

14) Klason C., Kubat J., *J Appl Polym Sci* **1975**, *19*: 831

15) Voet A., *Rubber Chem Technol* **1980**, *54*: 42

16) Allak H.K., Brinkman A.W., Woods J., *J Mater Sci* **1993**, *28*: 117

17) Jia S.J., Zhang Z.C., Fan Y.M., Weng H.M., Zhang X.F., Hang R.D.,

Eur Polym J **2002**, *38*: 2433

18) Feng J.Y., Chan C.M., *Polymer* **2000**, *41*: 4559

19) Tang H., Chen X.G., Luo Y.X., *Eur Polym J* **1997**, *33*: 1383

20) Manuela H.B., Franciose E.D., *Carbon* **2001**, *39*: 375

21) Luo Y.L., Wang G.C., Zhang B.Y., Zhang Z.P., *Eur Polym J* **1998**, *34*: 1221

22) Lee G.J., Suh K.D., Im S.S., *Polym Eng Sci* **1998**, *38*: 471

23) Zhang M.Y., Jia W.T., Chen X.F., *J Appl Polym Sci* **1996**, *62*: 743

24) Jia WT, Chen XF., *J Appl Polym Sci* **1994**, *54*: 1219

25) Jia W.T., Chen X.F., *J Appl Polym Sci* **1997**, *66*: 1885

26) Zhang M.Q., Yu G., Zeng H.M., Zhang H.B., Hou Y.H.,
    Macromolecules **1998**, *31*: 6724

27) Xu C., Agari Y., Matsuo M., *Polym J* **1998**, *30*: 372

28) Brandrup J., Immergut E.H., Grulke E.A.,
    Polymer handbook. 4th ed. New York: Wiley, **1999**

29) Tang H., Piao J.H., Chen X.F., Luo Y.X., Li S.H., *J Appl Polym Sci*., *48*: 1795 (1993)

30) Bueche F., *J appl phys* **1973**, *44*: 532

31) Chan C.M., Cheng C.L., Yuen M.M.F., *Polym Eng Sci*., *37*: 1127 (1997)

32) Y. Xi, H. Ishikawa, Y. Bin, M. Matsuo, Carbon 42, 1699 (2002)

33) Y. Xi, Y. Bin, C. K. Chiang and M. Matsuo, Carbon **45** 1303, (2007)

34) Hindermann-Bischoff M, Ehrburger-Dolle F., *Carbon*, *39*: 375 (2001)

35) Lee G J, Suh K D., *Polym Eng and Sci.*, *38*: 471 (1998)

36) H. Kawamoto. Carbon black-polymer composites,
    E.K. Sichel, editor, New York: Marcel Dekker, (1982)

37) Soares B G, Leyva M E, Barra G M O, Khastgir D., *Eur Polym J.*, *42*: 676 (2006)

38) Smyth C P., Dielectric behavior and structure.
    New York: McGram-Hill Book Company Inc., 191 (1955)

39) MćCrum, N G, Read B E, Williams G.   An elastic and dielectric effects in
    polymeric solids. New York: John Wiley& Sons, 211 (1967)

40) Ku CC, Liepins D. Electrical properties of polymers.
    Munich: Hanser Publishers, 34 (1987)

41) Macedo P B, Moynihan C T, Bose R., *Phys Chem Glasses*, *13*: 171 (1972)

42) Tsangaris G M, Psarras G C, Kouloumbi N., *J Mater Sc* ., *33*: 2027 (1998)

43) Wu G, Asai S, Zhang C, Miura T, Sumita M.,
    J Appl Phys., *88*: 1480 (2000)

Chapter IV

1) M. S. P. Shaffer, A. H. Windle, Adv. Mater. **11**, 937 (1999).

2) D. Qian, E. C. Dickey, R. Andrew, T. Rantell, Appl. Phys.Lett. **76**, 2868 (2000).

3) Z. Jia, Z. Wang, J. Liang, B. Wei, D.Wu, Mater. Sci. Eng. **271**, 395 (1999).

4) V. Lordi, N.Yao, J. Mater. Res. **15**, 2770 (2000).

5) P. Pötschke, A. R. Bhattacharyya, A. Janke, Polymer   **44**, 8061 (2003).

6) Safadi, R. Andrews, E. A. Grulke, J. Appl. Polym. Sci. **84**, 2660 (2002).

7) J. Yang, J. Hu, C. Wang, Y. Qin, Z. Guo, Macro. Mater. Eng. **289**, 828 (2004).

8) X. Jiang, Y. Bin, N. Kikyotani, M. Matsuo, Poly. J. **38**, 419 (2006).

9)Y. Tanaka, H. Nakanishi, S. Saeki, T.Yamaguchi, J. Appl. Phys. **37**, 4467 (1998).

10) P. K. Karanja, J. Polym. Mater. **22**, 369 (2005).

11) S. L. A. da Silva, M. L. A.Temperini, G. G. de Barros,
    J. Appl. Poly. Sci. **87**, 939 (2003).

12) X. Zeng, T. Ko, J. Poly. Sci. B. **35**, 1993 (1997).

13) G. G. de Barros, M. J. A. Sales, A. R. F.de Britto, Poly. Eng. Sci. **36**, 1125 (1996).

14) O. Jankovskij, V. Švorčik, V. Rybka, V. Hnatowicz,
    J. Appl. Poly. Sci. **60**, 1455 (1996).

15)J. N. Mutuku, P. K. Karanja, J. Polym. Mater. **20**, 445 (2003).

16) T. J. Lewis, D. M .Taylor, J. Phys. D: Appl. Phys. **5**, 1664 (1972).

17) W. Zhou, S. Xie, L. Sun, D. Tang, Y. Li, Z. Liu, L. Ci, X. Zou, G. Wang,
    Appl. Phys. Lett. **80**, 2553 (2002).

18) T. Michel, L. Alvarez, J. L. Sauvajol, R. Almairac, R. Aznar, O. Mathon, J. L.
    Bantignies, E. Flahaut, J. Phys. Chem. Soli. **67**, 1190 (2006).

19)A. M. Rao, P. C. Eklund, S. Bandow, A. Thess, R. E. Smalley,
    Nature. **388**, 257. 1997,

20) Y. Bin, M. Kitanaka, M. Matsuo, Macromolecules   **36**, 6213 (2003).

21) R. J. Nemanish, S. A. Solin, Phys. Rev. B. **20**, 392 (1979).

22) D. Stauffer, A. Aharony,
    Introduction to Percolation Theory. Taylor and Francis: London, 1994.

23) J. N. Coleman, S. Curran, A. P. Dalton, B. McCarthy, W. Blau, R. C. Barklie,
    Phys. Rev. B. **58**, 7492 (1998).

24) S. Rul, F. Lefèvre-schlick, E. Capria, Ch. Laurent, A. Peigney,

Acta Materialia. **52**, 1061 (2004).

25) S. Barrau, P. Demont, A. Peigney, Ch. Laurent, C. Lacabanne,
Macromolecules **36**, 5187 (2003).

26) M. Wber, M. R. Kamal, Poly. Comp. **18**, 711 (1997).

27) Y. Xi, H. Ishikawa, Y. Bin, M. Matsuo, Carbon **42**, 1699 (2004).

28) L. Grigorian, K. A. Williams, S. Fang, G. U. Sumanasekera, A. L. Loper, E. C.
Dickey, S. J. Pennycook, P. C. Eklund, Phys. Revi. Lett. **80**, 5560 (1998).

29) R. C. Teitelbaum, S. L. Ruby, T. J. Marks, J. Am. Chem. Soc. **101**, 7568 (1979).

30) T. Michel, L. Alvarez, J.-L. Sauvajol, R. Almairac, R. Aznar, O. Mathon, J,-L.
Bantignies, E. Flahaut, J. Phys. Chem. Solid. **67**, 1190 (2006).

31) M. Pigeon, R. E. Prudhomme, M. Pbzolet, Macromolecules **24**, 5687 (1991).

32) P. Karanjal, R. Nath,
IEEE Transactioiis on Dielectrics and Electrical Insulation **1**, 213 (1994).

33) D. K. Davies, J. Phys. D: Appl. Phys. **5**, 162 (1972).

34) J. Cambedouzou, J. L. Sauvajol, A. Rahmani, E. Flahaut, A. Peigney, C. Laurent,
Phys. Rew. B. **69**, 235422 (2004).

35) Q. Chen, Y. Bin, M. Matsuo, Macromolecules **39**, 6265 (2006)

36) Y. Bin, A. Yamanaka, Q. Chen, Y. Xi, X. Jiang, M. Matsuo, Polymer J. **39** 598
(2007)

37) J. Brandrup, E. H. Immergut, E. A. Grulke,
Polymer handbook.4th ed. New York: Wiley, 1999.

38) H. Kawai, T. Hashimoto, S. Suehiro, K. Fujita, Polym. Eng. Sci., **24** 361 (1984)

39) M. Matsuo, C. Sawatari, T. Ohhata, Macromolecules **21** 1317 (1988)

40) M. Matsuo, Y. Bin, C. Xu, L. Ma, T. Nakaoki, T. Suzuki, Polymer **44**, 4325 (2003)

41) M. Matsuo, L. Ma, M. Azuma, C. He, T. Suzuki, Macromolecules **35** 3059 (2002)